

16 **Abstract**

17

18 Meiotic crossover recombination is essential for both accurate chromosome segregation and the
19 generation of new haplotypes for natural selection to act upon. While the conserved role of the
20 ATPase, PCH-2, during meiotic prophase has been enigmatic, a universal phenotype that is observed
21 when *pch-2* or its orthologs are mutated is a change in the number and distribution of meiotic
22 crossovers. Here, we show that PCH-2 controls the number and distribution of crossovers by
23 antagonizing crossover formation. This antagonism produces different effects at different stages of
24 meiotic prophase: early in meiotic prophase, PCH-2 prevents double strand breaks from becoming
25 crossovers, limiting crossovers at sites of initial DSB formation and homolog interactions. Later in
26 meiotic prophase, PCH-2 winnows the number of crossover-eligible intermediates, contributing to the
27 reinforcement of crossover-eligible intermediates, designation of crossovers and ultimately, crossover
28 assurance. We also demonstrate that PCH-2 accomplishes this regulation through the meiotic
29 HORMAD, HIM-3. Our data strongly support a model in which PCH-2's conserved role is to remodel
30 meiotic HORMADs throughout meiotic prophase to destabilize crossover-eligible precursors,
31 coordinate meiotic recombination with synapsis, and contribute to the progressive implementation of
32 meiotic recombination, guaranteeing crossover control.

33 **Introduction**

34

35 Meiosis is a specialized type of cell division that reduces chromosome number by half, resulting in the
36 production of four genetically diverse haploid gametes, so that fertilization during sexual reproduction
37 restores diploidy. This process occurs in two stages: meiosis I, in which homologous chromosomes
38 are partitioned, and meiosis II, in which sister chromatid are segregated. The regulation of meiosis is
39 crucial for ensuring that both genetic recombination and chromosome segregation occur accurately.
40 During prophase I, homologous chromosomes pair and this pairing is stabilized through a process
41 called synapsis, in which a protein structure called the synaptonemal complex (SC) holds homologs
42 together. This close association between homologs during synapsis facilitates crossover formation, the
43 process in which double strand breaks (DSBs) are deliberately introduced into the genome, repaired
44 by meiosis-specific mechanisms that exchange DNA between homologous chromosomes and
45 generate the chiasmata, or linkage, that promotes accurate meiotic chromosome segregation.
46 Therefore, disruptions in pairing, synapsis, or recombination prevent the formation of chiasmata and
47 can lead to meiotic errors such as nondisjunction, resulting in aneuploid gametes. Errors in human
48 meiosis are associated with birth defects, such as Down and Turner syndromes, infertility and
49 miscarriages, underscoring the importance of understanding meiosis to human health (Hassold &
50 Hunt, 2001).

51

52 In addition to the fundamental role that recombination plays in ensuring accurate chromosome
53 segregation, crossover recombination accomplishes another important function: it generates new
54 haplotypes for natural selection to act upon to drive evolution. Thus, to assure a random assortment of
55 alleles on a population level, the distribution of crossovers may be as tightly regulated as their number.
56 The significance of controlling both crossover number and distribution is clearly illustrated by the
57 existence of mechanisms such as crossover assurance, in which every pair of homologous
58 chromosomes gets at least one crossover; crossover homeostasis, in which the number of crossovers
59 remains relatively invariant even if the number of recombination precursors change; and crossover

60 interference, in which the presence of a crossover inhibits the formation of a crossover nearby (Gray &
61 Cohen, 2016). DSBs typically vastly outnumber crossovers in most organisms and are introduced
62 gradually throughout early prophase. Therefore, to accomplish this precise level of control, meiotic
63 crossover recombination and the decision about which DSBs become crossover-eligible
64 intermediates, and eventually crossovers, is implemented progressively throughout meiotic prophase
65 (Cole et al., 2012; Joshi et al., 2015; Morgan et al., 2021; Yokoo et al., 2012).

66
67 PCH-2, also known as TRIP13 in mammals, is an evolutionarily ancient AAA-ATPase that plays a
68 significant role in regulating meiosis across different organisms, including *M. musculus* (mice), *S.*
69 *cerevisiae* (budding yeast), *D. melanogaster* (fruit flies), and *C. elegans* (worms) (Bhalla, 2023). PCH-
70 2 and its orthologs structurally remodel a family of proteins with HORMA domains (HORMADs) to
71 control their function (Gu et al., 2022). HORMADs participate in a variety of signaling events and can
72 exist in at least three structurally distinct conformations: a “closed” conformation, which they adopt
73 when they bind a short peptide sequence in their own protein sequence or another protein (also called
74 a closure motif) and their C-terminus wraps around this motif to stabilize the interaction; an “open”
75 conformation when unbound, in which their C-terminus is discretely tucked against the HORMA
76 domain; and an “extended” conformation, which is an intermediate between the two (Gu et al., 2022).
77 PCH-2 and its orthologs convert the closed version of HORMADs to the open or extended versions,
78 playing an important role in recycling HORMADs during signaling. During meiosis, closed versions of
79 meiotic HORMADs assemble on chromosomes to form meiotic chromosome axes, which are essential
80 for pairing, synapsis and recombination between homologous chromosomes (Kim et al., 2014). The
81 remodeling of meiotic HORMADs by PCH-2 to an “open” or “extended” conformation is thought to
82 reduce the levels of HORMADs on chromosomes (Börner et al., 2008; Cuacos et al., 2021; Lambing
83 et al., 2015; Wojtasz et al., 2009) and/or increase their dynamic association and dissociation (Russo et
84 al., 2023), modulating and coordinating homolog pairing, synapsis and recombination during
85 prophase.

86

87 The conserved role of the PCH-2/HORMAD module in meiosis has been difficult to characterize, in
88 part, we have argued, because of the evolutionary innovation that is an inherent aspect of sexual
89 reproduction (Bhalla, 2023). Moreover, in some systems, such as budding yeast and plants (Herruzo
90 et al., 2021; Yang et al., 2020), PCH-2 orthologs not only remodel meiotic HORMADs on meiotic
91 chromosomes but also perform this function in the cytoplasm to make meiotic HORMADs available for
92 their role(s) in meiotic nuclei. This dual role can complicate functional analyses, particularly in *pch-2*
93 null mutants. However, all meiotic systems exhibit defects in the number and distribution of crossovers
94 when PCH-2 function is abrogated by mutation (Deshong et al., 2014; Joshi et al., 2009; Joyce &
95 McKim, 2009; Lambing et al., 2015; Roig et al., 2010; Zanders & Alani, 2009). Unfortunately, the lack
96 of a clear pattern when analyzing these defects in recombination in *pch-2* mutants has contributed to
97 an inability to develop a unified, integrated model of PCH-2 function in the field.

98

99 In *C. elegans*, meiotic HORMADs localize to meiotic chromosomes independently of PCH-2 (Deshong
100 et al., 2014). Here, we exploit this system to show that PCH-2 is required to control the number and
101 distribution of crossovers by antagonizing the formation of crossovers. This antagonism produces
102 different consequences depending on the stage of meiotic prophase. In early meiotic prophase, PCH-
103 2 inhibits DSBs from becoming crossovers, ensuring that they are more widely distributed than sites of
104 initial DSB formation and/or homolog interactions. Later in meiotic prophase, PCH-2 is responsible for
105 winnowing the numbers of crossover-eligible intermediates on synapsed chromosomes, contributing
106 to the reinforcement of crossover-eligible intermediates, designation of crossovers and ultimately,
107 crossover assurance. Genetic analysis demonstrates that PCH-2's regulation of crossover-eligible
108 intermediates is through one of three essential meiotic HORMADs, HIM-3. Finally, we link PCH-2's
109 effect on early DSBs in early meiotic prophase to cell cycle stage, demonstrating that both limit early
110 DSBs from becoming crossovers. We propose that PCH-2's remodeling of HIM-3 on meiotic
111 chromosomes destabilizes crossover-eligible intermediates throughout meiotic prophase, contributing
112 to the progressive implementation of meiotic recombination to control the number and distribution of
113 crossovers and accomplish crossover control.

114

115 **Results**

116 **PCH-2 controls the number and distribution of crossovers in similar patterns on multiple** 117 **chromosomes**

118

119 We had previously shown that loss of PCH-2 reduced the frequency of double crossovers and genetic
120 length of both an autosome (chromosome III) and the X chromosome, albeit not uniformly among
121 genetic intervals (Deshong et al., 2014). To determine whether a more obvious pattern could be
122 observed, we expanded our analysis by monitoring recombination genetically in both wildtype and
123 *pch-2* mutant animals using five single nucleotide polymorphisms (SNPs) that spanned 95% of
124 Chromosomes, I, III, IV and the X chromosome (Figure 1). We excluded Chromosome II from our
125 analysis because of the potential difficulty combining Hawaiian SNPs with the *pch-2* mutation, which is
126 linked to Chromosome II, and Chromosome V because of our use of the *bcls39* transgene to identify
127 cross progeny, which may disrupt recombination on that chromosome.

128

129 In wildtype animals, we observed multiple double crossovers, ranging from 1-13 depending on the
130 chromosome. In a majority of these double crossovers (69%), one crossover was at the end of the
131 chromosome where pairing and synapsis initiate, also called the Pairing Center (PC) (MacQueen et
132 al., 2005), suggesting some relationship between where chromosomes might make initial contacts and
133 the likelihood of double crossovers. On all chromosomes analyzed, we observed no double
134 crossovers in *pch-2* mutants and this difference was statistically significant for Chromosomes I, III and
135 X. Moreover, there was a striking shift of crossovers to the PC end of all four chromosomes tested.
136 This shift in the distribution of crossovers to the PC ends of chromosomes was generally accompanied
137 by a reduction in crossovers in the center of chromosomes. In *C. elegans*, the center of chromosomes
138 are where double strand breaks are less numerous (Nadarajan et al., 2021; Yu et al., 2016) and where
139 genes are more abundant. In the case of the X chromosome and chromosome III, recombination at
140 the non-PC end was also reduced and appeared to more closely resemble the physical map at this

141 end of these chromosomes. Thus, PCH-2 ensures a wider distribution of crossovers across
142 chromosomes, away from regions that are more likely to undergo early homolog interactions (PC
143 ends) and with more double strand breaks (both the PC and non-PC ends of chromosomes), and
144 towards the center of chromosomes, where double strand breaks are less abundant.

145

146 **PCH-2 prevents exogenous DSBs early in meiotic prophase from becoming crossovers**

147

148 We previously showed that PCH-2 promotes crossover formation and crossover assurance through its
149 regulation of the meiotic HORMAD, HIM-3, in *C. elegans* (Russo et al., 2023). Moreover, this
150 promoting role seems linked to its localization to the synaptonemal complex (Patel et al., 2023).
151 However, the observed shift in the distribution of crossovers in *pch-2* mutants suggests that PCH-2
152 may also play a role in inhibiting crossovers and that this role may be occurring in early meiotic
153 prophase, when chromosomes are undergoing initial homolog interactions. Previous data from our lab
154 had suggested this possibility, but experimental caveats limited our ability to properly interpret these
155 experiments (Deshong et al., 2014).

156

157 To explicitly test this possibility, we took advantage of both the spatiotemporal organization of meiotic
158 nuclei in the *C. elegans* germline, and the observation that nuclei travel in an assembly line process at
159 a stereotypical pace to late pachytene (Jaramillo-Lambert et al., 2007), where we can cytologically
160 assess crossover formation by staining for the essential crossover factor, COSA-1 (Yokoo et al.,
161 2012). We performed irradiation experiments to introduce exogenous DSBs at different timepoints
162 during meiotic prophase and analyzed PCH-2's role in crossover formation (Figure 2A).

163

164 In this experiment, we tested the effects of ionizing radiation at two distinct time points: 8 hours after
165 irradiation, when we can monitor crossover formation in meiotic nuclei that received exogenous DSBs
166 in mid-pachytene, and 24 hours after irradiation, when we monitor crossover formation in meiotic

167 nuclei that received exogenous DSBs in leptotene/zygotene, also known as the transition zone in *C.*
168 *elegans*. In order to detect crossovers, control and *pch-2* mutants germlines were stained for
169 GFP::COSA-1, which allowed us to visualize crossovers, and DAPI, which allowed us to visualize
170 DNA. At 8 hours after irradiation, we observed a significant increase in nuclei containing less than 6
171 COSA-1 nuclei in *pch-2* mutants (26%), when compared to control (9%) germlines (Figure 2B, 2C).
172 We did not observe a significant number of nuclei with greater than 6 COSA-1 foci in either
173 backgrounds. This observation is consistent with our and others' previous findings: exogenous DSBs
174 in mid-pachytene do not affect the number of crossovers in wildtype animals (Yokoo et al., 2012) and
175 loss of PCH-2 leads to a decrease in crossover formation (Deshong et al., 2014).

176

177 Next, we examined crossover formation 24 hours post-irradiation (Figure 2D, 2E). For this time point,
178 we also saw a significant increase in nuclei containing less than 6 COSA-1 foci (control: 13%, *pch-2*:
179 26%), similar to the 8 hour time point. However, in contrast to the 8 hour time point, we also observed
180 a significant increase in nuclei with more than 6 COSA-1 foci in *pch-2* mutants (wildtype: 2%, *pch-2*:
181 13%), indicating that loss of PCH-2 leads to increased crossover formation when nuclei in the
182 transition zone get more DSBs. In other words, PCH-2 inhibits exogenous DSBs in early meiotic
183 prophase from becoming crossovers, consistent with our analysis of recombination on multiple
184 chromosomes.

185

186 **PCH-2 prevents SPO-11-induced DSBs from becoming crossovers in early meiotic prophase**

187

188 Our previous experiment indicated that PCH-2 is preventing exogenous DSBs in early meiotic
189 prophase from becoming crossovers (Figure 2). To test whether this was also the case for
190 programmed meiotic DSB formation, we used the auxin-inducible degradation (AID) system to remove
191 the enzyme that is responsible for programmed meiotic DSBs, SPO-11 (*spo-11::AID::3XFLAG*)
192 (Dernburg et al., 1998; Keeney et al., 1997). Since meiotic nuclei travel through the germline at about
193 one cell per row per hour (Jaramillo-Lambert et al., 2007), we took advantage of this precise

194 spatiotemporal resolution to test five different timepoints to determine if acute depletion of SPO-11
195 leads to any changes in crossover formation between control animals and *pch-2* mutants (Figure 3A).
196 We assayed crossover formation by analyzing both the number of GFP::COSA-1 foci in late
197 pachytene and the presence of bivalents in diakinesis, which indicates the successful formation of
198 chiasmata between homologous chromosomes. Meiotic nuclei travel from late pachytene to diakinesis
199 in approximately 12 hours (Deshong et al., 2014).

200

201 When we treated both control and *pch-2* mutant worms for 36 hours with auxin, we observed a
202 complete loss of GFP::COSA-1 foci (Figure 3C). When these animals were treated with auxin for 48
203 hours, to allow nuclei without SPO-11 an additional 12 hours to reach diakinesis, we observed 12
204 DAPI stained bodies, or univalents, which are the 6 homolog pairs that have not formed chiasmata
205 (Figure 3E). Thus, we can reliably remove SPO-11 from meiotic nuclei throughout the germline and
206 prevent crossover formation.

207

208 Having established that we can reliably remove SPO-11 with the AID system, we performed the same
209 experiment at additional timepoints that remove SPO-11 at different stages of early meiotic prophase,
210 monitoring crossover formation both at late pachytene and 12 hours later in diakinesis: 24 hours to
211 monitor GFP::COSA-1 foci and 36 hours to monitor bivalent formation; 22 (GFP::COSA-1 foci) and 34
212 (bivalent formation) hours; 20 (GFP::COSA-1 foci) and 32 hours (bivalent formation); and 18
213 (GFP::COSA-1 foci) and 30 hours (bivalent formation). We also performed a control experiment,
214 treating worms with ethanol for the 24 and 36 hour timepoints to ensure that this tagged version of
215 SPO-11 was fully functional for crossover formation (Figure 3C, 3D).

216

217 At the 24 hour time point, when meiotic nuclei in the transition zone do not receive SPO-11-induced
218 DSBs, we observe a range of GFP::COSA-1 foci in late pachytene in both control animals and *pch-2*
219 mutants with a majority of nuclei having 0 or 1 focus (control and *pch-2* averages: 1.8 GFP::COSA-1
220 foci), indicating a loss of crossover formation, albeit with some heterogeneity. This was confirmed

221 when we monitored bivalent formation at the 36 hour timepoint in both strains. This heterogeneity
222 likely reflects that it takes 1-4 hours to significantly affect DSB formation through acute degradation of
223 SPO-11 at this stage of meiosis in *C. elegans* (Hicks et al., 2022). In addition, there was no statistically
224 significant difference in the number of GFP::COSA-1 foci between control animals and *pch-2* mutants.
225 However, we did observe a slight, statistically significant difference in the number of DAPI stained
226 bodies between control animals (average number of DAPI stained bodies: 10.6) and *pch-2* mutants
227 (average number of DAPI stained bodies: 9.6), suggesting that even at this very early time point, we
228 can detect a role for PCH-2 in preventing early SPO-11-induced DSBs from becoming crossovers
229 (Figure 3D, 3E).

230

231 We continued to monitor GFP::COSA-1 and bivalent formation at successive timepoints. At the 22
232 hours and 34 hour timepoints, where SPO-11 depletion begins later in the transition zone, we saw an
233 increase in the number of GFP::COSA-1 foci and a reduction in the number of DAPI stained bodies,
234 suggesting that more DSBs are becoming crossovers. This trend continued at the 20 hour and 32 hour
235 timepoints, eventually reaching wildtype numbers for GFP::COSA-1 and DAPI stained bodies by the
236 18 hour and 30 hour timepoints, respectively.

237

238 At the 22 hour and 36 hour timepoints, we did not detect any statistically significant difference in the
239 number of GFP::COSA-1 foci or DAPI stained bodies between control animals and *pch-2* mutants,
240 even when we analyzed the number of nuclei that had greater than 6 GFP::COSA-1 foci. In contrast,
241 while the number of GFP::COSA-1 foci was not statistically significantly different between control
242 animals and *pch-2* mutants at the 20 hour time point, the number of nuclei with greater than 6
243 GFP::COSA-1 foci was significantly higher in *pch-2* mutants (control: 3%, *pch-2*: 10%, p value =
244 0.009, Fischer's Exact Test), similar to our analysis of GFP::COSA-1 24 hours after irradiation. Even
245 more strikingly, the number of DAPI stained bodies was significantly lower in *pch-2* animals than
246 control animals at the corresponding 32 hour timepoint, indicating that more homolog pairs had
247 successfully formed chiasmata in *pch-2* mutants. The inconsistency between the average number of

248 GFP::COSA-1 foci and DAPI stained bodies at this time point can be explained by our ability to more
249 reliably detect *pch-2*'s loss of crossover assurance when quantifying GFP::COSA-1 foci than when
250 analyzing bivalent formation (Deshong et al., 2014; Russo et al., 2023). No difference in GFP::COSA-
251 1 foci or bivalent formation was observed at the 18 hour and 30 hours timepoints, respectively. These
252 data indicate that during a narrow time frame of early meiotic prophase, likely during
253 leptotene/zygotene given the delay in limiting DSB formation with auxin-induced degradation of SPO-
254 11, PCH-2 prevents SPO-11-induced DSBs from becoming crossovers and chiasmata.

255

256 **PCH-2 is required for timely loading and removal of MSH-5 on meiotic chromosomes through**
257 **its regulation of HIM-3**

258

259 After DSB formation, a subset of DSBs are repaired through a pro-crossover pathway and eventually
260 winnowed to a stereotypical number of crossovers. In *C. elegans*, this can be visualized by the loading
261 of the pro-crossover factor MSH-5, a component of the meiosis-specific MutS γ complex that
262 stabilizes crossover-specific DNA repair intermediates called joint molecules (Janisiw et al., 2018;
263 Kelly et al., 2000; Snowden et al., 2004). GFP::MSH-5 begins to form a few foci in the transition zone,
264 becoming more numerous in early pachytene before decreasing in number in mid pachytene to
265 ultimately colocalize with COSA-1 marked sites in late pachytene (Janisiw et al., 2018; Woglar &
266 Villeneuve, 2018; see control in Figure 4A, 4B). The mechanism through which MSH-5 functions with
267 the SC and other meiosis factors to ultimately form crossovers has not been established but may
268 involve phosphorylation by cyclin-dependent kinases (Haversat et al., 2022; Zhang et al., 2021).

269

270 Given that we have shown that PCH-2 prevents early DSBs from becoming crossovers (Figures 2 and
271 3), we tested whether we could cytologically detect this inhibition at the level of MSH-5 behavior in
272 control animals and *pch-2* mutants. We generated wildtype and *pch-2* mutants with GFP::MSH-5 and
273 quantified the average number of GFP::MSH-5 foci per row of nuclei from the transition zone to late

274 pachytene (Figure 4A, 4B). We observed a statistically significant increase in the average number of
275 GFP::MSH-5 foci per row in the transition zone in *pch-2* mutants (Figure 4A, 4B, p value < 0.0001,
276 Student's t-test), indicating that PCH-2 typically limits MSH-5 loading at this early stage of meiotic
277 prophase. The average number of GFP::MSH-5 foci per row were similar in number in early pachytene
278 in both backgrounds. However, we also observed a substantial increase in the average number of
279 GFP::MSH-5 foci per row in *pch-2* mutants in the mid and late pachytene regions (Figure 4A, 4B),
280 indicating that PCH-2 also promotes the turnover or maturation of GFP::MSH-5 foci at these later
281 stages of meiotic prophase. Thus, PCH-2 prevents the loading of the crossover-promoting factor,
282 MSH-5, during early meiotic prophase, consistent with both our genetic analysis of recombination
283 (Figure 1) and its role in preventing early DSBs from becoming crossovers (Figures 2 and 3).
284 However, PCH-2 also appears to limit the number of crossover-eligible intermediates in mid and late
285 pachytene, an unexpected observation given that the most severe recombination defect in *pch-2*
286 mutants is the loss of crossover assurance (Deshong et al., 2014).

287

288 We previously showed that PCH-2 genetically interacts with meiotic HORMADs to effectively control
289 different aspects of meiosis: PCH-2 regulates pairing and synapsis through its regulation of HTP-3 and
290 crossover recombination through its regulation of HIM-3 (Russo et al., 2023). To determine which
291 meiotic HORMAD PCH-2 might be regulating to affect GFP::MSH-5's loading and removal on meiotic
292 chromosomes, we constructed *gfp::msh-5;htp-3^{H96Y}*, *gfp::msh-5;pch-2;htp-3^{H96Y}*, *gfp::msh-5;him-3^{R93Y}*
293 and *gfp::msh-5;pch-2;him-3^{R93Y}* mutants and quantified GFP::MSH-5 foci throughout the germline.
294 Both *htp-3^{H96Y}* and *him-3^{R93Y}* mutants showed a drastic increase in the average number of GFP::MSH-
295 5 per row of nuclei throughout the germline (Figures 4C and 4D, Supplemental Figure 1). For
296 example, compared to control germlines that peaked at approximately an average of 20 MSH-5 foci
297 per row in early pachytene and then decreased in mid-pachytene, *him-3^{R93Y}* germlines had closer to
298 an average of 30 GFP::MSH-5 foci per row in early pachytene. Moreover, the average number of
299 GFP::MSH-5 foci per row increased further in mid and late pachytene, achieving peaks closer to an
300 average of 35 foci (Figure 4D). These very high numbers of GFP::MSH-5 were striking but do not

301 produce an increased number of crossovers in *htp-3^{H96Y}* or *him-3^{R93Y}* single mutants (Russo et al.,
302 2023), raising the possibility that not all of them reflect functional, crossover-specific intermediates,
303 similar to what has been observed in the absence of synapsis (Woglar & Villeneuve, 2018). These
304 data also suggest that these mutations, which disrupt the ability of meiotic HORMADs to adopt the
305 “closed” conformation (Russo et al., 2023), affect the behavior of GFP::MSH-5 on meiotic
306 chromosomes.

307

308 Quantification of GFP::MSH-5 foci in *pch-2;htp-3^{H93Y}* double mutants was similar to *htp-3^{H93Y}* single
309 mutants, suggesting that PCH-2’s effect on the behavior of GFP::MSH-5 foci was not through its
310 regulation of HTP-3 (Supplemental Figure 1). In stark contrast to *pch-2;htp-3^{H93Y}* double mutants, the
311 *pch-2;him-3^{R93Y}* double mutant showed a dramatic decrease in the overall average of MSH-5 foci per
312 row throughout the germline (Figure 4C, 4D). These averages fell between the averages in control and
313 *pch-2* mutant animals, particularly in the transition zone and late pachytene (Figure 4D), consistent
314 with our previous report that this double mutant has fewer defects in crossover formation than either
315 single mutant (Russo et al., 2023). These data indicate that PCH-2’s effect on promoting the removal
316 of GFP::MSH-5 in both the transition zone and mid to late pachytene is through its regulation of HIM-
317 3.

318

319 *pch-2* single mutants exhibit a loss of crossover assurance (Deshong et al., 2014). However, our
320 quantification of GFP::MSH-5 in *pch-2* single mutants in mid to late pachytene showed an increased
321 number of crossover-eligible intermediates (Figure 4A, 4B), suggesting a complex relationship
322 between having too many crossover-eligible intermediates and crossover assurance in *C. elegans*. To
323 address this inconsistency, we generated strains with both OLLAS::COSA-1 (Janisiw et al., 2018) and
324 GFP::MSH-5 in wildtype animals and *pch-2* mutants. Consistent with our and others’ previous findings,
325 we observe a gradual reduction in the average number of GFP::MSH-5 foci per row of nuclei in control
326 animals as these nuclei approach the end of pachytene, ultimately converging with the average

327 number of OLLAS::COSA-1 foci per row (Figure 4E, 4F) (Janisiw et al., 2018; Woglar & Villeneuve,
328 2018). In addition, we consistently observed co-localization of GFP::MSH-5 and OLLAS::COSA-1 foci
329 in control animals, with a few MSH-5 foci persisting without COSA-1 (Figure 4E, 4F).

330

331 By contrast, we detected higher average numbers of GFP::MSH-5 foci per row across all late
332 pachytene nuclei in *pch-2* mutants and this average never converged upon the average number of
333 OLLAS-1::COSA-1 foci per row (Figure 4E, 4F). To test whether there was a correlation between the
334 number of GFP::MSH-5 foci and the loss of crossover assurance in *pch-2* mutants, we determined the
335 average number of GFP::MSH-5 foci in meiotic nuclei with 6 OLLAS::COSA-1 foci and those with less
336 than 6 OLLAS::COSA-1 foci in both control and *pch-2* mutant animals (Figure 4E, 4G, Supplemental
337 Figure 2). Indeed, we observed that *pch-2* mutant nuclei with less than 6 OLLAS::COSA-1 foci had
338 significantly higher numbers of GFP::MSH-5 foci, compared to both control and *pch-2* mutant nuclei
339 with 6 OLLAS::COSA-1 foci (Figure 4E, 4G), suggesting that the inability to reduce the number of
340 crossover-eligible intermediates in *pch-2* mutants, counterintuitively, contributes to the observed loss
341 of crossover assurance.

342

343 **PCH-2 is removed from the synaptonemal complex when crossovers are designated**

344

345 We have previously shown that PCH-2 localization to the SC is extended when there are partial
346 defects in synapsis or changes in karyotype, producing an increase in crossovers and a loss of
347 crossover interference (Deshong et al. 2014; Patel et al., 2023). These data led us to hypothesize that
348 PCH-2's presence on chromosomes promotes crossover formation. However, our quantification of
349 GFP::MSH-5 indicates that PCH-2 is required to limit the number of crossover-eligible intermediates,
350 in direct contrast to our proposed hypothesis (Figure 4). Therefore, we decided to revisit what role
351 PCH-2 localization to the SC might play in regulating crossover formation. To this end, we localized
352 PCH-2 in *dsb-2* mutants, in which DSB formation is substantially reduced and fewer crossovers are
353 formed in *C. elegans* (Rosu et al., 2013). We performed this experiment because, in budding yeast,

354 similar mutants that reduce DSB formation rely on Pch2 to successfully complete meiosis (Joshi et al.,
355 2009; Zanders & Alani, 2009).

356

357 Because the recombination defect in *dsb-2* mutants worsens with age (Rosu et al., 2013), we looked
358 at PCH-2 localization in both young (24 hours post L4 larval stage) and older animals (48 hours post
359 L4). We observed a unique and striking localization pattern in *dsb-2* mutants that we had not observed
360 before. When stained for PCH-2 and GFP::*COSA-1*, nuclei retain PCH-2 onto chromosomes far into
361 late pachytene, past the normal region when PCH-2 typically is removed from chromosomes (Figure
362 5A, 5B). However, unlike what we have observed in other mutants that have defects in synapsis or
363 changes in karyotype, this retention of PCH-2 is not uniform among all late pachytene nuclei in *dsb-2*
364 mutants. Instead, most nuclei lose PCH-2 localization in late pachytene while some retain it. We
365 tested whether there was a relationship between the retention of PCH-2 and the number of
366 GFP::*COSA-1* foci and found that 96% of nuclei that lose PCH-2 have at least 1 GFP::*COSA-1* focus
367 (Figure 5A, 5B). In older animals (see 48 hours post-L4), this pattern was even more clear: 77% of
368 nuclei without PCH-2 had 1 or more GFP::*COSA-1* focus and 93% of meiotic nuclei without a
369 GFP::*COSA-1* focus retained PCH-2.

370

371 These data indicate that PCH-2's removal from the SC is in response to, coincident with or facilitates
372 crossover designation. To distinguish between these possibilities, we analyzed GFP::*COSA-1* foci in
373 *dsb-2::AID* (Zhang et al., 2018) and *dsb-2::AID;pch-2* worms, reasoning that if PCH-2's removal is in
374 response to or coincident with designation, we should not detect any differences in the number of
375 GFP::*COSA-1* foci in *dsb-2::AID* and *dsb-2::AID;pch-2* worms. We performed these experiments with
376 the auxin-inducible degradation system because of variability in the *dsb-2* mutant background that
377 affected reproducibility of our experiments.

378

379 Upon auxin treatment of *dsb-2::AID* worms, we observed a statistically significant (p value < 0.0001,
380 Mann-Whitney U test) decrease in the number of GFP::COSA-1 foci, in comparison with ethanol-
381 treated worms, verifying that we can reliably knock down DSB-2 with the AID system (Figure 5D).
382 When we performed the same experiment in *dsb-2::AID;pch-2* worms, the average number of
383 GFP::COSA-1 foci further decreased, indicating that fewer crossovers are designated when DSBs are
384 reduced and PCH-2 is absent (Figure 5C, 5D). These data suggest that PCH-2's presence on the SC
385 prevents crossover designation. Given the correlation between elevated GFP::MSH-5 foci and the loss
386 of crossover assurance we observe in *pch-2* mutants, we propose that PCH-2 is retained on meiotic
387 chromosomes to ensure that extra crossover-eligible intermediates are removed and crossover
388 designation is delayed until crossover assurance can be guaranteed in *C. elegans*.

389 390 **PCH-2 and high CHK-2 activity control the fate of early double strand breaks**

391
392 In *C. elegans*, meiotic cell cycle entry and progression depends on the activity of CHK-2, the meiosis-
393 specific ortholog of the DNA-damage kinase Chk2/CHEK2 (Baudrimont et al., 2022; Castellano-Pozo
394 et al., 2020; Kim et al., 2015; MacQueen & Villeneuve, 2001; Zhang et al., 2023). Meiotic nuclei in
395 leptotene/zygotene are characterized by high CHK-2 activity, which drops to intermediate activity in
396 mid-pachytene (Kim et al., 2015; Zhang et al., 2023). In late pachytene, CHK-2 activity is inactivated
397 by the recruitment of polo-like kinase, PLK-2, to the SC, which enables crossover designation (Zhang
398 et al., 2023). Thus, CHK-2 activity also has consequences for the progression of meiotic
399 recombination and DNA repair.

400
401 Given that early DSBs are prevented from becoming crossovers by PCH-2 in early meiotic prophase,
402 we wanted to test if high CHK-2 activity in leptotene/zygotene also contributed to the fate of these
403 early DSBs. To evaluate this possibility, we used *syp-1^{T452A}* mutants (Sato-Carlton et al., 2018). The
404 SC component, SYP-1, is phosphorylated by CDK-1 on T452, producing a Polo box binding motif that
405 recruits PLK-2 to the SC, contributing to the inactivation of CHK-2 when chromosomes are synapsed

406 (Brandt et al., 2020; Zhang et al., 2023). Therefore, in *syp-1^{T452A}* mutants, CHK-2 activity remains high
407 throughout most of meiotic prophase in the *C. elegans* germline (Figure 6A).

408

409 We quantified the total number of GFP::COSA-1 foci in late pachytene nuclei in *syp-1^{T452A}* mutants
410 and observed a significant decrease in the average number of GFP::COSA-1 foci when compared to
411 control animals (Figures 6B and 6C), consistent with previous findings that *syp-1^{T452A}* mutants delay
412 designation and have fewer crossovers (Zhang et al., 2023). These data are also consistent with the
413 possibility that some DSBs fail to become crossovers when CHK-2 activity remains high. If this
414 hypothesis is correct, we predict that the combination of high CHK-2 activity and loss of *pch-2* should
415 produce more crossovers. We generated *pch-2;syp-1^{T452A}* double mutants to test this hypothesis.
416 When we quantified GFP::COSA-1 in *pch-2;syp-1^{T452A}* double mutants, we detected a significant
417 increase in the average number of GFP::COSA-1 foci compared to *syp-1^{T452A}* single mutants (Figure
418 6C), in strong support of our hypothesis.

419

420 To further verify that the *pch-2* mutation suppresses the crossover defect in *syp-1^{T452A}* mutants, we
421 also monitored bivalent formation in diakinesis nuclei. *syp-1^{T452A}* single mutants exhibit an average of
422 7.12 DAPI staining bodies in diakinesis, higher than both control animals and *pch-2* single mutants
423 (Figure 6D). By contrast, *pch-2;syp-1^{T452A}* mutants had an average of 6.05 DAPI staining bodies
424 (Figure 6D, 6E), directly supporting our COSA-1 analysis and indicating that both PCH-2 function and
425 high CHK-2 activity collaborate to control the fate of DSBs and prevent some of them from becoming
426 crossovers in early meiotic prophase.

427

428 Discussion

429

430 We have shown that PCH-2 antagonizes crossover formation throughout meiotic prophase and that
431 this regulation occurs through one of the three essential meiotic HORMADs in *C. elegans*, HIM-3

432 (Figure 4). We propose that PCH-2 remodels HIM-3 on meiotic chromosomes to destabilize
433 crossover-eligible intermediates, thus limiting which DSBs will become crossovers (Figure 7).
434 However, this antagonism has different consequences depending on when during meiotic prophase it
435 occurs, underscoring the importance of temporal regulation of these events. During
436 leptotene/zygotene, when CHK-2 activity is high (Kim et al., 2015; Zhang et al., 2023) and PCH-2 is
437 present as foci on chromosomes (Deshong et al., 2014), PCH-2 prevents crossover formation at some
438 sites of initial DSB formation and early homolog interactions (Figure 7B). In this way, PCH-2 promotes
439 a wider distribution of crossovers across the genome (Figure 1). In pachytene, when CHK-2 activity
440 has decreased (Kim et al., 2015; Zhang et al., 2023) and PCH-2 is localized to the SC (Deshong et al.,
441 2014), PCH-2 winnows crossover-eligible intermediates, ensuring their reinforcement, designation and
442 crossover assurance (Figure 7B). When there are defects in recombination, such as partial synapsis
443 (Deshong et al., 2014), changes in karyotype (Patel et al., 2023) or too few DSBs (Figure 5), PCH-2
444 persists on the SC to prevent designation, guarantee crossover assurance and some degree of
445 homeostasis, independent of an additional feedback mechanism that increases DSB formation (Patel
446 et al., 2023). That persistence of PCH-2 also disrupts crossover interference in two of these situations
447 (Deshong et al., 2014; Patel et al., 2023) strongly suggests that crossover interference is
448 mechanistically linked to assurance and homeostasis.

449
450 *him-3^{R93Y};**pch-2* double mutants have stronger crossover assurance than either single mutant but less
451 than wildtype animals (Russo et al., 2023), a phenotype which can now be explained by the behavior
452 of GFP::MSH-5 foci in these double mutants (Figure 4C, 4D). We have shown that HIM-3^{R93Y} mutant
453 protein can adopt the closed conformation and loads on meiotic chromosomes similar to wildtype HIM-
454 3 (Russo et al. 2023). In vitro analysis shows that HIM-3^{R93Y} binds its closure motif with reduced
455 affinity, likely affecting its ability to adopt the closed conformation in vivo (Figure 7A and Russo et al.
456 2023). The proposed role of PCH-2 in meiosis is to remodel meiotic HORMADs from the closed
457 conformation to the extended one (Figure 7A), regulating their association with chromosomes (Bhalla,
458 2023). However, since meiotic HORMADs are not visibly depleted from chromosomes during meiotic

459 progression in *C. elegans* (Couteau et al., 2004; Couteau & Zetka, 2005; Goodyer et al., 2008;
460 Martinez-Perez & Villeneuve, 2005), this genetic interaction supports a role for PCH-2 in temporarily
461 reducing the occupancy of meiotic HORMADs on meiotic chromosomes, destabilizing interactions with
462 partner proteins that modulate the progression and fidelity of meiotic recombination (Russo et al.,
463 2023). Thus, PCH-2's remodeling of HIM-3 would disrupt protein-protein interactions that underlie
464 crossover-eligible intermediates, destabilizing them and reducing their number on chromosomes,
465 contributing to crossover control (Figure 7B). Since meiotic HORMADs are essential for meiotic
466 chromosome axis structure and function, our data therefore support a role for the meiotic axis in
467 crossover control, as suggested by previous reports (Chu et al., 2024; Girard et al., 2023; Lambing et
468 al., 2020; Nabeshima et al., 2004). However, the disassembly of crossover-eligible intermediates
469 would also release pro-crossover factors present at these sites to concentrate at other, more stable
470 sites on the SC, contributing to reinforcement and designation during synapsis (Girard et al., 2023;
471 Yokoo et al., 2012). Moreover, these results raise the possibility that this behavior of PCH-2 and/or
472 meiotic HORMADs might be regulated by post-translational modifications associated with crossover
473 control, such as ubiquitination, SUMOylation and phosphorylation (Gray & Cohen, 2016).

474

475 Given that mutation of PCH-2 produces changes in the number and distribution of crossovers across
476 multiple model systems, we argue that controlling crossover distribution and number is the conserved
477 role of PCH-2 in meiosis (Bhalla, 2023). We have previously proposed that the conserved role of PCH-
478 2 is to coordinate meiotic recombination with synapsis (Bhalla, 2023). With these results, we further
479 refine this model. Early in meiotic prophase, PCH-2 remodels meiotic HORMADs to prevent some
480 DSBs from becoming crossover-eligible intermediates, widening the recombination landscape beyond
481 early homolog interactions and/or sites that tend to be more favorable for DSB formation, also known
482 as 'hot spots.' For example, this may explain the localization of TRIP13, the PCH-2 ortholog in mice,
483 to telomeres (Chotiner et al., 2024), sites that experience early homolog interactions due to the
484 organization of meiotic chromosomes in the bouquet formation (Scherthan et al., 1996). This
485 antagonism may also expand the regions of the genome that initiate synapsis in organisms that use

486 DSBs to accomplish this event. This possibility is supported by the observation that loss of TRIP13 in
487 mammals produce meiotic chromosomes that exhibit partial asynapsis (Roig et al., 2010), particularly
488 near regions that may act as barriers to SC polymerization (Brown et al., 2005; Roig et al., 2010).
489 Limiting which DSBs becomes crossover-eligible intermediates in early meiotic prophase also ensures
490 that meiotic recombination overlaps with synapsis, either completely, as in *C. elegans* (Yokoo et al.,
491 2012) or partially, as in budding yeast, plants and mice (Capilla-Perez et al., 2021; Cole et al., 2012;
492 Joshi et al., 2015; Morgan et al., 2021). Once synapsis is complete, PCH-2 continues to remodel
493 meiotic HORMADs on chromosomes to control the gradual implementation of crossover number and
494 distribution, reinforcing the important role that synapsis plays in mediating crossover control (Durand
495 et al., 2022; Libuda et al., 2013).

496

497 Unexpectedly, the inability to reduce the number of crossover-eligible intermediates in *pch-2* mutants,
498 as visualized by GFP::MSH-5 foci, does not produce extra crossovers but a loss of crossover-
499 assurance in *C. elegans* (Figure 4), a somewhat counterintuitive result. One interpretation of these
500 data is that crossover-eligible intermediates may be more numerous but absent from some
501 chromosomes in *pch-2* mutants, explaining the loss of crossover assurance. Since the absence of
502 crossover intermediates in *C. elegans* is accompanied by premature desynapsis of individual
503 chromosomes (Machovina et al., 2016; Pattabiraman et al., 2017) and chromosomes in *pch-2* mutants
504 delay desynapsis (Deshong et al., 2014), we do not favor this interpretation. Instead, we propose that
505 having too many crossover-eligible intermediates can be as deleterious to crossover assurance as
506 having too few (Figure 7B). This possibility is further supported by the loss of crossover assurance we
507 detect in irradiated wildtype worms, which is exacerbated in *pch-2* mutants (Figure 2).

508

509 This phenomenon, where crossover-eligible intermediates need to be winnowed to some threshold
510 number to ensure crossover assurance, may also explain the loss of crossover assurance also
511 observed in *Trip13* deficient mice (Roig et al., 2010) and on small chromosomes in budding yeast

512 (Chakraborty et al., 2017). Alternatively, the counterintuitive relationship between the number of
513 crossover-eligible precursors and crossover assurance in *pch-2* mutants we observe might reflect an
514 additional layer of regulation during crossover formation specific to *C. elegans*. Since *C. elegans*
515 chromosomes are holocentric, crossovers play an additional role organizing chromosomes for the
516 ordered release of sister chromatid cohesion during meiosis I (Martinez-Perez et al., 2008; Nabeshima
517 et al., 2005) and extra crossovers can be deleterious to accurate chromosome segregation (Hollis et
518 al., 2020). By contrast, in *Arabidopsis*, a system that appears to be able to tolerate an extraordinarily
519 high number of crossovers with little to no effect on chromosome segregation (Durand et al., 2022),
520 PCH2's inability to localize to the SC produces an increase in crossover formation (Figure 7), as
521 visualized by both MLH1 foci and the formation of chiasmata (Yang et al., 2022). Once again, an
522 overarching theme that becomes apparent in our model is that PCH-2 may play a common role in
523 different systems, with dramatic variations in phenotypic consequences given species-specific
524 requirements and constraints.

525

526 We were not surprised to see high numbers of double crossovers on almost every chromosome in our
527 genetic analysis of recombination in wildtype worms, given our previous analysis (Deshong et al.,
528 2014). However, we were surprised to see that the majority of them were found near Pairing Centers
529 and sites of synapsis initiation, suggesting a relationship between early homolog interactions and the
530 formation of double crossovers. When we revisited our previous data, we observed similar patterns. In
531 addition, we do not detect these double crossovers cytologically in *C. elegans*, even when using the
532 OLLAS::COSA-1 reporter, which has been reported to identify double crossovers in spermatogenesis
533 not visualized by GFP::COSA-1 (Cahoon et al., 2023). Crossovers that are cytologically marked by
534 COSA-1 are known as Class I crossovers, which depend on pro-crossover factors such as MSH-5 and
535 ZHP-3, and exhibit crossover control (Gray & Cohen, 2016). These data raise the intriguing possibility
536 that these double crossovers are the product of the alternate, Class II, pathway of crossover
537 formation, which relies on a different suite of proteins, does not respond to crossover control and

538 contributes to varying degrees in different model systems (Gray & Cohen, 2016; Youds et al., 2010).
539 Thus, important corollaries of our model may be that PCH-2 specifically coordinates recombination
540 with synapsis to promote Class I crossovers, limit Class II crossovers and that Class II crossovers are
541 more likely to form early in meiosis, prior to synapsis. Therefore, variations in the contribution of the
542 Class II crossover pathways to crossover recombination and the degree of cross-talk between Class I
543 and Class II pathways among model systems might reflect the degree to which crossover formation
544 overlaps with synapsis (Bhalla, 2023; Gray & Cohen, 2016; Yokoo et al., 2012). Furthermore, these
545 corollaries are entirely consistent with PCH-2's absence from the genome of fission yeast (Wu &
546 Burgess, 2007), a system in which chromosomes do not undergo synapsis, crossovers do not exhibit
547 interference and all crossovers are dependent on the Class II pathway (Hollingsworth & Brill, 2004).
548
549 Our results also have some additional important implications about the regulation of DSB formation
550 across the genome in *C. elegans*. We explain the shift in the recombination landscape away from the
551 central regions of chromosomes and toward PC ends in *pch-2* mutants (Figure 1) as a result of early
552 DSBs becoming crossovers at the expense of later DSBs, suggesting that when DSBs happen in
553 meiotic prophase affects where they happen in the genome. Specifically, we propose that
554 chromosome arms, which are gene poor, receive DSBs early during (or even throughout) DSB
555 formation and the center of chromosomes, which are gene rich, receive DSBs later. A similar
556 regulation of the timing of DSB formation has been demonstrated in budding yeast, where the DSB
557 landscape across the whole genome expands when time in prophase is increased (López Ruiz et al.,
558 2024) and small, highly recombinogenic, chromosomes, get more DSBs later in meiotic prophase
559 (Murakami et al., 2020; Subramanian et al., 2019). However, this temporal regulation has not been
560 reported previously in *C. elegans* and suggests that this phenomenon is more widely conserved. This
561 expansion of the DSB landscape in *C. elegans* to include the center regions of chromosomes later in
562 meiosis may be a deliberate attempt for recombination to create new haplotypes for evolution to act
563 on, despite the relative paucity of DSBs and the observation that they can result in chromosome
564 missegregation (Altendorfer et al., 2020).

565

566 Finally, our work raises some important questions about the functional role(s) of DSBs in meiosis,
567 aside from their contributions to crossover formation. Hicks and colleagues were the first to report that
568 early DSBs do not contribute to crossover formation in *C. elegans* (Hicks et al., 2022). Here we show
569 that these early DSBs are prevented from becoming crossovers by both PCH-2 activity and cell cycle
570 stage, specifically in leptotene/zygotene, when homologs are initiating pairing and synapsis. In
571 budding yeast, similar, early-occurring DSBs have been characterized as “scout DSBs” because of
572 their preference for repair from sister chromatids, versus homologous chromosomes, and their
573 proposed role in contributing to homolog pairing (Borde & de Massy, 2015; Joshi et al., 2015). The
574 homolog bias that these “scout DSBs” do display seems dependent on budding yeast *PCH2* (Joshi et
575 al., 2015) but interpreting this experiment is complicated by the fact that Pch2 is also required to make
576 the budding yeast meiotic HORMAD, Hop1, available for its loading onto meiotic chromosomes
577 (Herruzo et al., 2021).

578

579 In contrast to budding yeast, *C. elegans* does not rely on DSBs to promote homolog pairing and
580 initiate synapsis (Dernburg et al., 1998); in worms, *cis*-acting sites called Pairing Centers are essential
581 for homolog pairing and synapsis (MacQueen et al., 2005). There is certainly some support in the
582 literature for DSBs playing a role in supporting pairing and synapsis in *C. elegans* (Guo et al., 2022;
583 Mlynarczyk-Evans et al., 2013; Roelens et al., 2015). However, if these early DSBs were contributing
584 to pairing and synapsis, we would expect to see a genetic interaction between *htp-3^{H96Y}* and *pch-2*
585 mutations in the installation of GFP::MSH-5 in the transition zone; we previously reported that *htp-*
586 *3^{H96Y}* suppresses the acceleration of pairing and synapsis of *pch-2* mutants, particularly when Pairing
587 Center function is compromised (Russo et al., 2023). Instead, we favor the possibility that these early
588 DSBs are generated to amplify the signaling of DNA damage kinases to prime them for their role in
589 recombination, a role that has also been proposed for “scout” DSBs (Joshi et al., 2015). That ATM-1, a
590 conserved DNA damage kinase that is downstream of CHK-2 in *C. elegans*, relies on DSBs for full
591 activity, supports this proposed, conserved role (Yu et al., 2023).

592

593 Our work provides an important framework to finally understand the role of PCH-2 in controlling the
594 number and distribution of crossovers, a role that we argue is its conserved role. While specific details
595 may vary across systems, we propose that PCH-2 remodels meiotic HORMADs throughout meiotic
596 prophase to destabilize crossover-eligible precursors, coordinating meiotic recombination with
597 synapsis, contributing to the progressive implementation of meiotic recombination and guaranteeing
598 crossover assurance, interference and homeostasis.

599

600 **Methods and Materials**

601

602 ***C.elegans* Genetics and Genome Engineering**

603 The *C. elegans* Bristol N2 was used as the wild-type strain. All strains were maintained at 20°C under
604 standard conditions unless stated. Mutant combinations were generated by crossing. The following
605 mutants and rearrangements were used:

606

607 *LGII: pch-2(tm1458), mels8 ([pie-1p::GFP::cosa-1 + unc-119(+)], dsb-2(me96), dsb-2(ie58[dsb-*
608 *2::AID::3xFLAG])*

609

610 *LGIII: cosa-1(DDR12[OLLAS::cosa-1]); htp-3(vc75)*

611

612 *LGIV: him-3(blt9), spo-11(ie59[spo-11::AID::3xFLAG]), msh-5[DDR22(GFP::msh-5)], ieSi38 [sun-*
613 *1p::TIR1::mRuby::sun-1 3'UTR + Cbr-unc-119(+)]*

614

615 *LGV: syp-1(icm85[T452A]), nT1[qIs51], bcls39 (Plin-15::ced-1::GFP)*

616

617 **Genetic analysis of Recombination**

618 The wildtype Hawaiian CB4856 strain (HI) and the Bristol N2 strain were used to assay recombination
619 between single nucleotide polymorphisms (SNPs) on Chromosomes I, III, IV and X (Wicks et al.,
620 2001; Bazan et al., 2011). The SNPs, primers, enzymes used for restriction digests and expected
621 fragment sizes are included in Supplemental Table 1. To measure wild-type recombination, N2 males
622 containing *bcls39* were crossed to Hawaiian CB4856 worms. Cross-progeny hermaphrodites were
623 identified by the presence of *bcls39* and contained one N2 and one CB4856 chromosome.

624

625 These were assayed for recombination by crossing with CB4856 males containing *myo-2::mCherry*.
626 Cross-progeny hermaphrodites from the resulting cross were isolated as L4s, and then cultured
627 individually in 96- well plates in liquid S-media complete supplemented with HB101. Four days after
628 initial culturing, starved populations were lysed and used for PCR and restriction digest to detect N2
629 and CB4856 SNP alleles. For recombination in *pch-2* mutants, strains homozygous for the CB4856
630 background of the relevant SNPs were created, then mated with *pch-2; bcls39*. Subsequent steps
631 were performed as in the wild-type worms.

632

633 **Immunostaining**

634 DAPI staining and immunostaining was performed as in (Russo et al. 2023), 20 to 24 hours post L4
635 unless otherwise noted. For analyzing bivalents, the same protocol was implemented with the
636 exception that hermaphrodites were dissected and DAPI stained 48 hours post late L4 stage, unless
637 otherwise noted.

638

639 The following primary antibodies were used at the indicated dilutions: alpaca anti-GFP Booster
640 (ChromoTek, gb2AF488) was used at 1:1000; rat anti-OLLAS (Invitrogen, PIMA516125) was used at
641 1:1000; and rabbit anti PCH-2 (Bhalla 2014) was used at 1:500. The following secondary antibodies
642 were used at the indicated dilutions: anti-rabbit Cy3 (Jackson Labs) was used at 1:500 and anti-rat
643 Cy5 (Jackson Labs) was used at 1:500

644

645 **Irradiation Experiments**

646 Control and *pch-2* mutant L4's were aged 12-14 hours before being exposed to 1,000 rad (10 Gy) of
647 X-ray radiation using a Precision MultiRad 160 X-irradiator (Precision X-Ray Inc.). Germlines were
648 then fixed and stained, 8 hours and 24 hours post irradiation.

649

650 **Auxin-induced Degradation Experiments**

651 Auxin treatment was performed by transferring young adult worms (aged 12-14 hours post-L4) to
652 bacteria-seeded plates containing auxin or 99% ethanol at specific time points, except for experiments
653 in which L4s were transferred directly to bacteria-seeded plates containing auxin or ethanol (the 36
654 hour and 48 hour time points in Figures 3C and E and the experiments in Figures 5C and D). The
655 natural auxin indole3-acetic acid (IAA) was purchased from Alfa Aesar (#A10556). A 400 mM stock
656 solution in ethanol was prepared and was stored at 4°C for up to one month. Auxin was diluted to
657 100mM, and 100ul was spread onto NGM plates. Plates were allowed to dry before seeding with fresh
658 OP50 culture. Plates were left at 20°C for 2-3 days in the dark to allow for bacterial lawn growth.

659

660 **Imaging and Quantification**

661 All images were acquired using a DeltaVision Personal DV system (Applied Precision) equipped with a
662 100X N.A. 1.40 oil-immersion objective (Olympus), resulting in an effective XY pixel spacing of 0.064
663 or 0.040 µm. Three-dimensional image stacks were collected at 0.2-µm Z spacing and processed by
664 constrained, iterative deconvolution. Image scaling, analysis and maximum-intensity projections were
665 performed using functions in the softWoRx software package.

666

667 For analysis of GFP::*MSH-5* foci, sum projections were generated using ImageJ for each image of the
668 germline. ImageJ plugins Cell Counter, ROI Manager, and Find Maxima were used to identify and
669 quantify GFP::*MSH-5* foci by row from transition zone to the end of pachytene. The threshold value
670 was set depending on background conditions to ensure minimal signals were identified. Foci were

671 only quantified if they co-localized with DAPI staining. For all genotypes, three germlines per genotype
672 were analyzed and representative germlines are shown.

673

674 **Graphing and Statistical Analysis**

675 Data was analyzed using Python 3.8 and Prism for statistical significance. All datasets were tested for
676 normality using the Shapiro-Wilk test. For Figures 1, 2 and 5B, Fisher's exact test was used to
677 determine significance. For Figures 3, 4, 5D and 6, Mann-Whitney U test was used to determine
678 significance.

679

680 **Author contributions**

681 B.P., M.G., and N.B. designed the experiments. B.P., M.G., A.H., E.L., and V.O. performed the
682 experiments. B.P. and N.B. analyzed the data. B.P. and N.B. wrote the initial draft of the manuscript
683 and B.P., M.G., A.H. and N.B. revised the manuscript. N.B. acquired funding.

684

685 **Acknowledgements**

686 We would like to thank Josh Arribere, Pete Carlton, Abby Dernburg, Nicola Silva and Anne Villeneuve
687 for valuable strains and reagents. We would also like to thank the members of the Bhalla lab for
688 careful review of the manuscript. This work was supported by the NIH (grant numbers R35GM141835
689 [N.B.], R25GM051765 [V.O.] and T34GM140956 (A.H. and V.O.)). Some strains were provided by the
690 CGC, which is funded by NIH Office of Research Infrastructure Programs (P40 OD010440).

691

692 **References**

- 693 Altendorfer, E., Láscarez-Lagunas, L. I., Nadarajan, S., Mathieson, I., & Colaiácovo, M. P. (2020).
694 Crossover Position Drives Chromosome Remodeling for Accurate Meiotic Chromosome Segregation.
695 *Current Biology*, 30(7), 1329-1338.e7. <https://doi.org/10.1016/j.cub.2020.01.079>
696
- 697 Baudrimont, A., Paouneskou, D., Mohammad, A., Lichtenberger, R., Blundon, J., Kim, Y., Hartl, M.,
698 Falk, S., Schedl, T., & Jantsch, V. (2022). Release of CHK-2 from PPM-1.D anchorage schedules
699 meiotic entry. *Science Advances*, 8(7), eabl8861. <https://doi.org/10.1126/sciadv.abl8861>
700
- 701 Bhalla, N. (2023). PCH-2 and meiotic HORMADs: A module for evolutionary innovation in meiosis? *In*
702 *Current Topics in Developmental Biology* (Vol. 151, pp. 317–344). Elsevier.
703 <https://doi.org/10.1016/bs.ctdb.2022.07.001>
704
- 705 Borde, V., & deMassy, B. (2015). Meiosis: Early DNA Double-Strand Breaks Pave the Way for Inter-
706 Homolog Repair. *Developmental Cell*, 32(6), 663–664. <https://doi.org/10.1016/j.devcel.2015.03.011>
707
- 708 Börner, G. V., Barot, A., & Kleckner, N. (2008). Yeast Pch2 promotes domainal axis organization,
709 timely recombination progression, and arrest of defective recombinosomes during meiosis.
710 *Proceedings of the National Academy of Sciences*, 105(9), 3327–3332.
711 <https://doi.org/10.1073/pnas.0711864105>
712
- 713 Brandt, J. N., Hussey, K. A., & Kim, Y. (2020). Spatial and temporal control of targeting Polo-like
714 kinase during meiotic prophase. *Journal of Cell Biology*, 219(11), e202006094.
715 <https://doi.org/10.1083/jcb.202006094>
716

- 717 Brown, P. W., Judis, L., Chan, E. R., Schwartz, S., Seftel, A., Thomas, A., & Hassold, T. J. (2005).
718 Meiotic Synapsis Proceeds from a Limited Number of Subtelomeric Sites in the Human Male. *The*
719 *American Journal of Human Genetics*, 77(4), 556–566. <https://doi.org/10.1086/468188>
720
- 721 Cahoon CK, Uebel CJ, Villeneuve AM, Libuda DE. Epitope tag-specific differences in the detection of
722 COSA-1 marked crossover sites in *C. elegans* spermatocytes. *MicroPubl Biol.* 2023 Jan
723 6;2023:10.17912/micropub.biology.000724. <https://doi.org/10.17912/micropub.biology.000724>.
724
- 725 Capilla-Pérez, L., Durand, S., Hurel, A., Lian, Q., Chambon, A., Taochy, C., Solier, V., Grelon, M., &
726 Mercier, R. (2021). The synaptonemal complex imposes crossover interference and heterochiasmy in
727 *Arabidopsis*. *Proceedings of the National Academy of Sciences*, 118(12), e2023613118.
728 <https://doi.org/10.1073/pnas.2023613118>
729
- 730 Castellano-Pozo, M., Pacheco, S., Sioutas, G., Jaso-Tamame, A. L., Dore, M. H., Karimi, M. M., &
731 Martinez-Perez, E. (2020). Surveillance of cohesin-supported chromosome structure controls meiotic
732 progression. *Nature Communications*, 11(1), 4345. <https://doi.org/10.1038/s41467-020-18219-9>
733
- 734 Chakraborty, P., Pankajam, A. V., Lin, G., Dutta, A., Krishnaprasad, G. N., Tekkedil, M. M., Shinohara,
735 A., Steinmetz, L. M., & Nishant, K. T. (2017). Modulating Crossover Frequency and Interference for
736 Obligate Crossovers in *Saccharomyces cerevisiae* Meiosis. *Genes/Genomes/Genetics*, 7(5), 1511–
737 1524. <https://doi.org/10.1534/g3.117.040071>
738
- 739 Chotiner, J. Y., Leu, N. A., Yang, F., Cossu, I. G., Guan, Y., Lin, H., & Wang, P. J. (2024). TRIP13
740 localizes to synapsed chromosomes and functions as a dosage-sensitive regulator of meiosis.
741 <https://doi.org/10.7554/eLife.92195.2>
742
743

- 744 Chu, L., Zhuang, J., Geng, M., Zhang, Y., Zhu, J., Zhang, C., Schnittger, A., Yi, B., & Yang, C. (2024).
745 ASYNAPSIS3 has diverse dosage-dependent effects on meiotic crossover formation in *Brassica*
746 *napus*. *The Plant Cell*, koae207. <https://doi.org/10.1093/plcell/koae207>
747
- 748 Cole, F., Kauppi, L., Lange, J., Roig, I., Wang, R., Keeney, S., & Jasin, M. (2012). Homeostatic control
749 of recombination is implemented progressively in mouse meiosis. *Nature Cell Biology*, 14(4), 424–
750 430. <https://doi.org/10.1038/ncb2451>
751
- 752 Couteau, F., Nabeshima, K., Villeneuve, A., & Zetka, M. (2004). A Component of *C. elegans* Meiotic
753 Chromosome Axes at the Interface of Homolog Alignment, Synapsis, Nuclear Reorganization, and
754 Recombination. *Current Biology*, 14(7), 585–592. <https://doi.org/10.1016/j.cub.2004.03.033>
755
- 756 Couteau, F., & Zetka, M. (2005). HTP-1 coordinates synaptonemal complex assembly with homolog
757 alignment during meiosis in *C. elegans*. *Genes & Development*, 19(22), 2744–2756.
758 <https://doi.org/10.1101/gad.1348205>
759
- 760 Cuacos, M., Lambing, C., Pachon-Penalba, M., Osman, K., Armstrong, S. J., Henderson, I. R.,
761 Sanchez-Moran, E., Franklin, F. C. H., & Heckmann, S. (2021). Meiotic chromosome axis remodelling
762 is critical for meiotic recombination in *Brassica rapa*. *Journal of Experimental Botany*, 72(8), 3012–
763 3027. <https://doi.org/10.1093/jxb/erab035>
764
- 765 Dernburg, A. F., McDonald, K., Moulder, G., Barstead, R., Dresser, M., & Villeneuve, A. M. (1998).
766 Meiotic Recombination in *C. elegans* Initiates by a Conserved Mechanism and Is Dispensable for
767 Homologous Chromosome Synapsis. *Cell*, 94(3), 387–398. <https://doi.org/10.1016/S0092->
768 8674(00)81481-6
769

- 770 Deshong, A. J., Ye, A. L., Lamelza, P., & Bhalla, N. (2014). A Quality Control Mechanism Coordinates
771 Meiotic Prophase Events to Promote Crossover Assurance. *PLoS Genetics*, 10(4), e1004291.
772 <https://doi.org/10.1371/journal.pgen.1004291>
773
- 774 Durand, S., Lian, Q., Jing, J., Ernst, M., Grelon, M., Zwicker, D., & Mercier, R. (2022). Joint control of
775 meiotic crossover patterning by the synaptonemal complex and HEI10 dosage. *Nature*
776 *Communications*, 13(1), 5999. <https://doi.org/10.1038/s41467-022-33472-w>
777
- 778 Girard, C., Zwicker, D., & Mercier, R. (2023). The regulation of meiotic crossover distribution: A coarse
779 solution to a century-old mystery? *Biochemical Society Transactions*, 51(3), 1179–1190.
780 <https://doi.org/10.1042/BST20221329>
781
- 782 Goodyer, W., Kaitna, S., Couteau, F., Ward, J. D., Boulton, S. J., & Zetka, M. (2008). HTP-3 Links
783 DSB Formation with Homolog Pairing and Crossing Over during *C. elegans* Meiosis. *Developmental*
784 *Cell*, 14(2), 263–274. <https://doi.org/10.1016/j.devcel.2007.11.016>
785
- 786 Gray, S., & Cohen, P. E. (2016). Control of Meiotic Crossovers: From Double-Strand Break Formation
787 to Designation. *Annual Review of Genetics*, 50(1), 175–210. [https://doi.org/10.1146/annurev-genet-](https://doi.org/10.1146/annurev-genet-120215-035111)
788 [120215-035111](https://doi.org/10.1146/annurev-genet-120215-035111)
789
- 790 Gu, Y., Desai, A., & Corbett, K. D. (2022). Evolutionary Dynamics and Molecular Mechanisms of
791 HORMA Domain Protein Signaling. *Annual Review of Biochemistry*, 91(1), 541–569.
792 <https://doi.org/10.1146/annurev-biochem-090920-103246>
793
- 794 Guo, H., Stamper, E. L., Sato-Carlton, A., Shimazoe, M. A., Li, X., Zhang, L., Stevens, L., Jacky Tam,
795 K., Dernburg, A. F., & Carlton, P. M. (2022). Phosphoregulation of DSB-1 mediates control of meiotic
796 double-strand break activity. *eLife*, 11, e77956. <https://doi.org/10.7554/eLife.77956>

797

798 Hassold, T., & Hunt, P. (2001). To err (meiotically) is human: The genesis of human aneuploidy. *Nature*
799 *Reviews Genetics*, 2(4), 280–291. <https://doi.org/10.1038/35066065>

800

801 Haversat, J., Woglar, A., Klatt, K., Akerib, C. C., Roberts, V., Chen, S.-Y., Arur, S., Villeneuve, A. M., &
802 Kim, Y. (2022). Robust designation of meiotic crossover sites by CDK-2 through phosphorylation of the
803 MutSy complex. *Proceedings of the National Academy of Sciences*, 119(21), e2117865119.

804 <https://doi.org/10.1073/pnas.2117865119>

805

806 Herruzo, E., Lago-Maciel, A., Baztán, S., Santos, B., Carballo, J. A., & San-Segundo, P. A. (2021).
807 Pch2 orchestrates the meiotic recombination checkpoint from the cytoplasm. *PLOS Genetics*, 17(7),
808 e1009560. <https://doi.org/10.1371/journal.pgen.1009560>

809

810 Hicks, T., Trivedi, S., Eppert, M., Bowman, R., Tian, H., Dafalla, A., Crahan, C., Smolikove, S., & Silva,
811 N. (2022). Continuous double-strand break induction and their differential processing sustain chiasma
812 formation during *Caenorhabditis elegans* meiosis. *Cell Reports*, 40(13), 111403.

813 <https://doi.org/10.1016/j.celrep.2022.111403>

814

815 Hollingsworth, N. M., & Brill, S. J. (2004). The Mus81 solution to resolution: Generating meiotic
816 crossovers without Holliday junctions. *Genes & Development*, 18(2), 117–125.

817 <https://doi.org/10.1101/gad.1165904>

818

819 Hollis, J. A., Glover, M. L., Schlientz, A. J., Cahoon, C. K., Bowerman, B., Wignall, S. M., & Libuda, D.
820 E. (2020). Excess crossovers impede faithful meiotic chromosome segregation in *C. elegans*. *PLOS*
821 *Genetics*, 16(9), e1009001. <https://doi.org/10.1371/journal.pgen.1009001>

822

- 823 Janisiw, E., Dello Stritto, M. R., Jantsch, V., & Silva, N. (2018). BRCA1-BARD1 associate with the
824 synaptonemal complex and pro-crossover factors and influence RAD-51 dynamics during
825 *Caenorhabditis elegans* meiosis. *PLOS Genetics*, 14(11), e1007653.
826 <https://doi.org/10.1371/journal.pgen.1007653>
827
- 828 Jaramillo-Lambert, A., Ellefson, M., Villeneuve, A. M., & Engebrecht, J. (2007). Differential timing of S
829 phases, X chromosome replication, and meiotic prophase in the *C. elegans* germ line. *Developmental*
830 *Biology*, 308(1), 206–221. <https://doi.org/10.1016/j.ydbio.2007.05.019>
831
- 832 Joshi, N., Barot, A., Jamison, C., & Börner, G. V. (2009). Pch2 Links Chromosome Axis Remodeling at
833 Future Crossover Sites and Crossover Distribution during Yeast Meiosis. *PLOS Genetics*, 5(7),
834 e1000557. <https://doi.org/10.1371/journal.pgen.1000557>
835
- 836 Joshi, N., Brown, M. S., Bishop, D. K., & Börner, G. V. (2015). Gradual Implementation of the Meiotic
837 Recombination Program via Checkpoint Pathways Controlled by Global DSB Levels. *Molecular Cell*,
838 57(5), 797–811. <https://doi.org/10.1016/j.molcel.2014.12.027>
839
- 840 Joyce, E. F., & McKim, K. S. (2009). *Drosophila* PCH2 Is Required for a Pachytene Checkpoint That
841 Monitors Double-Strand-Break-Independent Events Leading to Meiotic Crossover Formation.
842 *Genetics*, 181(1), 39–51. <https://doi.org/10.1534/genetics.108.093112>
843
- 844 Keeney S, Giroux CN, Kleckner N. Meiosis-specific DNA double-strand breaks are catalyzed by
845 Spo11, a member of a widely conserved protein family. *Cell*. 1997 Feb 7;88(3):375-84. doi:
846 10.1016/s0092-8674(00)81876-0. PMID: 9039264.
847

848 Kelly, K. O., Dernburg, A. F., Stanfield, G. M., & Villeneuve, A. M. (2000). *Caenorhabditis elegans* msh-
849 5 Is Required for Both Normal and Radiation-Induced Meiotic Crossing Over but Not for Completion of
850 Meiosis. *Genetics*, 156(2), 617–630. <https://doi.org/10.1093/genetics/156.2.617>
851

852 Kim, Y., Kostow, N., & Dernburg, A. F. (2015). The Chromosome Axis Mediates Feedback Control of
853 CHK-2 to Ensure Crossover Formation in *C. elegans*. *Developmental Cell*, 35(2), 247–261.
854 <https://doi.org/10.1016/j.devcel.2015.09.021>
855

856 Kim, Y., Rosenberg, S. C., Kugel, C. L., Kostow, N., Rog, O., Davydov, V., Su, T. Y., Dernburg, A. F., &
857 Corbett, K. D. (2014). The Chromosome Axis Controls Meiotic Events through a Hierarchical Assembly
858 of HORMA Domain Proteins. *Developmental Cell*, 31(4), 487–502.
859 <https://doi.org/10.1016/j.devcel.2014.09.013>
860

861 Lambing, C., Kuo, P. C., Tock, A. J., Topp, S. D., & Henderson, I. R. (2020). ASY1 acts as a dosage-
862 dependent antagonist of telomere-led recombination and mediates crossover interference in
863 *Arabidopsis*. *Proceedings of the National Academy of Sciences*, 117(24), 13647–13658.
864 <https://doi.org/10.1073/pnas.1921055117>
865

866 Lambing, C., Osman, K., Nuntasontorn, K., West, A., Higgins, J. D., Copenhaver, G. P., Yang, J.,
867 Armstrong, S. J., Mechtler, K., Roitinger, E., & Franklin, F. C. H. (2015). *Arabidopsis* PCH2 Mediates
868 Meiotic Chromosome Remodeling and Maturation of Crossovers. *PLOS Genetics*, 11(7), e1005372.
869 <https://doi.org/10.1371/journal.pgen.1005372>
870

871 Libuda, D. E., Uzawa, S., Meyer, B. J., & Villeneuve, A. M. (2013). Meiotic chromosome structures
872 constrain and respond to designation of crossover sites. *Nature*, 502(7473), 703–706.
873 <https://doi.org/10.1038/nature12577>
874

- 875 López Ruiz, L. M., Johnson, D., Gittens, W. H., Brown, G. G. B., Allison, R. M., & Neale, M. J. (2024).
876 Meiotic prophase length modulates Tel1-dependent DNA double-strand break interference. *PLOS*
877 *Genetics*, 20(3), e1011140. <https://doi.org/10.1371/journal.pgen.1011140>
878
- 879 Machovina, T. S., Mainpal, R., Daryabeigi, A., McGovern, O., Paouneskou, D., Labella, S., Zetka, M.,
880 Jantsch, V., Yanowitz, J. L. (2016). A Surveillance System Ensures Crossover Formation in
881 *C. elegans*. *Current Biology*, 26(21), 2873-2884. <https://doi.org/10.1016/j.cub.2016.09.007>
882
- 883 MacQueen, A. J., Phillips, C. M., Bhalla, N., Weiser, P., Villeneuve, A. M., & Dernburg, A. F. (2005).
884 Chromosome Sites Play Dual Roles to Establish Homologous Synapsis during Meiosis in *C. elegans*.
885 *Cell*, 123(6), 1037–1050. <https://doi.org/10.1016/j.cell.2005.09.034>
886
- 887 MacQueen, A. J., & Villeneuve, A. M. (2001). Nuclear reorganization and homologous chromosome
888 pairing during meiotic prophase require *C. elegans chk-2*. *Genes & Development*, 15(13), 1674–1687.
889 <https://doi.org/10.1101/gad.902601>
890
- 891 Martinez-Perez, E., Schvarzstein, M., Barroso, C., Lightfoot, J., Dernburg, A. F., & Villeneuve, A. M.
892 (2008). Crossovers trigger a remodeling of meiotic chromosome axis composition that is linked to two-
893 step loss of sister chromatid cohesion. *Genes & Development*, 22(20), 2886–2901.
894 <https://doi.org/10.1101/gad.1694108>
895
- 896 Martinez-Perez, E., & Villeneuve, A. M. (2005). HTP-1-dependent constraints coordinate homolog
897 pairing and synapsis and promote chiasma formation during *C. elegans* meiosis. *Genes &*
898 *Development*, 19(22), 2727–2743. <https://doi.org/10.1101/gad.1338505>
899

- 900 Mlynarczyk-Evans, S., Roelens, B., & Villeneuve, A. M. (2013). Evidence That Masking of Synapsis
901 Imperfections Counterbalances Quality Control to Promote Efficient Meiosis. *PLoS Genetics*, 9(12),
902 e1003963. <https://doi.org/10.1371/journal.pgen.1003963>
903
- 904 Morgan, C., White, M. A., Franklin, F. C. H., Zickler, D., Kleckner, N., & Bomblies, K. (2021). Evolution
905 of crossover interference enables stable autopolyploidy by ensuring pairwise partner connections in
906 *Arabidopsis arenosa*. *Current Biology*, 31(21), 4713-4726.e4.
907 <https://doi.org/10.1016/j.cub.2021.08.028>
908
- 909 Murakami, H., Lam, I., Huang, P.-C., Song, J., Van Overbeek, M., & Keeney, S. (2020). Multilayered
910 mechanisms ensure that short chromosomes recombine in meiosis. *Nature*, 582(7810), 124–128.
911 <https://doi.org/10.1038/s41586-020-2248-2>
912
- 913 Nabeshima, K., Villeneuve, A. M., & Colaiácovo, M. P. (2005). Crossing over is coupled to late meiotic
914 prophase bivalent differentiation through asymmetric disassembly of the SC. *The Journal of Cell*
915 *Biology*, 168(5), 683–689. <https://doi.org/10.1083/jcb.200410144>
916
- 917 Nabeshima, K., Villeneuve, A. M., & Hillers, K. J. (2004). Chromosome-Wide Regulation of Meiotic
918 Crossover Formation in *Caenorhabditis elegans* Requires Properly Assembled Chromosome Axes.
919 *Genetics*, 168(3), 1275–1292. <https://doi.org/10.1534/genetics.104.030700>
920
- 921 Nadarajan, S., Altendorfer, E., Saito, T. T., Martinez-Garcia, M., & Colaiácovo, M. P. (2021). HIM-17
922 regulates the position of recombination events and GSP-1/2 localization to establish short arm identity
923 on bivalents in meiosis. *Proceedings of the National Academy of Sciences*, 118(17), e2016363118.
924 <https://doi.org/10.1073/pnas.2016363118>
925

- 926 Patel, B; Grobler, M; Bhalla, N (2023). Chromosomal fusions, but not chromosomal inversions,
927 activate a PCH-2 dependent checkpoint that promotes crossover formation in *C. elegans*.
928 *microPublication Biology*.
- 929
- 930 Pattabiraman, D., Roelens, B., Woglar, A., Villeneuve A. M. (2017) Meiotic recombination modulates
931 the structure and dynamics of the synaptonemal complex during *C. elegans* meiosis. *PLOS Genetics*,
932 13(3), e1006670. <https://doi.org/10.1371/journal.pgen.1006670>
- 933
- 934 Roelens, B., Schvarzstein, M., & Villeneuve, A. M. (2015). Manipulation of Karyotype in
935 *Caenorhabditis elegans* Reveals Multiple Inputs Driving Pairwise Chromosome Synapsis During
936 Meiosis. *Genetics*, 201(4), 1363–1379. <https://doi.org/10.1534/genetics.115.182279>
- 937
- 938 Roig, I., Dowdle, J. A., Toth, A., de Rooij, D. G., Jasin, M., & Keeney, S. (2010). Mouse TRIP13/PCH2
939 Is Required for Recombination and Normal Higher-Order Chromosome Structure during Meiosis.
940 *PLOS Genetics*, 6(8), e1001062. <https://doi.org/10.1371/journal.pgen.1001062>
- 941
- 942 Rosu, S., Zawadzki, K. A., Stamper, E. L., Libuda, D. E., Reese, A. L., Dernburg, A. F., & Villeneuve, A.
943 M. (2013). The *C. elegans* DSB-2 Protein Reveals a Regulatory Network that Controls Competence
944 for Meiotic DSB Formation and Promotes Crossover Assurance. *PLOS Genetics*, 9(8), e1003674.
945 <https://doi.org/10.1371/journal.pgen.1003674>
- 946
- 947 Russo, A. E., Giacomazzi, S., Deshong, A., Menon, M., Ortiz, V., Ego, K. M., Corbett, K. D., & Bhalla,
948 N. (2023). The conserved AAA ATPase PCH-2 distributes its regulation of meiotic prophase events
949 through multiple meiotic HORMADs in *C. elegans*. *PLOS Genetics*, 19(4), e1010708.
950 <https://doi.org/10.1371/journal.pgen.1010708>
- 951
- 952 Sato-Carlton, A., Nakamura-Tabuchi, C., Chartrand, S. K., Uchino, T., & Carlton, P. M. (2018).

- 953 Phosphorylation of the synaptonemal complex protein SYP-1 promotes meiotic chromosome
954 segregation. *Journal of Cell Biology*, 217(2), 555–570. <https://doi.org/10.1083/jcb.201707161>
955
- 956 Scherthan, H., Weich, S., Schwegler, H., Heyting, C., Härle, M., & Cremer, T. (1996). Centromere and
957 telomere movements during early meiotic prophase of mouse and man are associated with the onset
958 of chromosome pairing. *The Journal of Cell Biology*, 134(5), 1109–1125.
959 <https://doi.org/10.1083/jcb.134.5.1109>
960
- 961 Snowden, T., Acharya, S., Butz, C., Berardini, M., & Fishel, R. (2004). hMSH4-hMSH5 Recognizes
962 Holliday Junctions and Forms a Meiosis-Specific Sliding Clamp that Embraces Homologous
963 Chromosomes. *Molecular Cell*, 15(3), 437–451. <https://doi.org/10.1016/j.molcel.2004.06.040>
964
- 965 Subramanian, V. V., Zhu, X., Markowitz, T. E., Vale-Silva, L. A., San-Segundo, P. A., Hollingsworth, N.
966 M., Keeney, S., & Hochwagen, A. (2019). Persistent DNA-break potential near telomeres increases
967 initiation of meiotic recombination on short chromosomes. *Nature Communications*, 10(1), 970.
968 <https://doi.org/10.1038/s41467-019-08875-x>
969
- 970 Wicks, S. R., Yeh, R. T., Gish, W. R., Waterston, R. H., & Plasterk, R. H. A. (2001). Rapid gene
971 mapping in *Caenorhabditis elegans* using a high density polymorphism map. *Nature Genetics*, 28(2),
972 160–164. <https://doi.org/10.1038/88878>
973
- 974 Woglar, A., & Villeneuve, A. M. (2018). Dynamic Architecture of DNA Repair Complexes and the
975 Synaptonemal Complex at Sites of Meiotic Recombination. *Cell*, 173(7), 1678-1691.e16.
976 <https://doi.org/10.1016/j.cell.2018.03.066>
- 977 Wojtasz, L., Daniel, K., Roig, I., Bolcun-Filas, E., Xu, H., Boonsanay, V., Eckmann, C. R., Cooke, H. J.,
978 Jasin, M., Keeney, S., McKay, M. J., & Toth, A. (2009). Mouse HORMAD1 and HORMAD2, Two

- 979 Conserved Meiotic Chromosomal Proteins, Are Depleted from Synapsed Chromosome Axes with the
980 Help of TRIP13 AAA-ATPase. *PLOS Genetics*, 5(10), e1000702.
981 <https://doi.org/10.1371/journal.pgen.1000702>
982
- 983 Wu, H. Y., & Burgess, S. M. (2006). Two distinct surveillance mechanisms monitor meiotic
984 chromosome metabolism in budding yeast. *Current biology: CB*, 16(24), 2473–2479.
985 <https://doi.org/10.1016/j.cub.2006.10.069>
986
- 987 Yang, C., Hu, B., Portheine, S. M., Chuenban, P., & Schnittger, A. (2020). State changes of the
988 HORMA protein ASY1 are mediated by an interplay between its closure motif and PCH2. *Nucleic
989 Acids Research*, 48(20), 11521-11535. <https://doi.org/10.1093/nar/gkaa527>
990
- 991 Yang, C., Sofroni, K., Hamamura, Y., Hu, B., Elbasi, H. T., Balboni, M., Chu, L., Stang, D., Heese, M.,
992 & Schnittger, A. (2022). ZYP1-mediated recruitment of PCH2 to the synaptonemal complex remodels
993 the chromosome axis leading to crossover restriction. *Nucleic Acids Research*, 50(22), 12924–12937.
994 <https://doi.org/10.1093/nar/gkac1160>
995
- 996 Yokoo, R., Zawadzki, K. A., Nabeshima, K., Drake, M., Arur, S., & Villeneuve, A. M. (2012). COSA-1
997 Reveals Robust Homeostasis and Separable Licensing and Reinforcement Steps Governing Meiotic
998 Crossovers. *Cell*, 149(1), 75–87. <https://doi.org/10.1016/j.cell.2012.01.052>
999
- 1000 Youds, J. L., Mets, D. G., McIlwraith, M. J., Martin, J. S., Ward, J. D., O'Neil, N. J., Rose, A. M., West,
1001 S. C., Meyer, B. J., & Boulton, S. J. (2010). RTEL-1 Enforces Meiotic Crossover Interference and
1002 Homeostasis. *Science*, 327(5970), 1254–1258. <https://doi.org/10.1126/science.1183112>
1003

- 1004 Yu, Z., Kim, H. J., & Dernburg, A. F. (2023). ATM signaling modulates cohesin behavior in meiotic
1005 prophase and proliferating cells. *Nature Structural & Molecular Biology*, 30(4), 436–450.
1006 <https://doi.org/10.1038/s41594-023-00929-5>
1007
- 1008 Yu, Z., Kim, Y., & Dernburg, A. F. (2016). Meiotic recombination and the crossover assurance
1009 checkpoint in *Caenorhabditis elegans*. *Seminars in Cell & Developmental Biology*, 54, 106–116.
1010 <https://doi.org/10.1016/j.semcdb.2016.03.014>
1011
- 1012 Zanders, S., & Alani, E. (2009). The *pch2Δ* Mutation in Baker's Yeast Alters Meiotic Crossover Levels
1013 and Confers a Defect in Crossover Interference. *PLOS Genetics*, 5(7), e1000571.
1014 <https://doi.org/10.1371/journal.pgen.1000571>
1015
- 1016 Zhang, L., Köhler, S., Rillo-Bohn, R., & Dernburg, A. F. (2018). A compartmentalized signaling network
1017 mediates crossover control in meiosis. *eLife*, 7, e30789. <https://doi.org/10.7554/eLife.30789>
1018
- 1019 Zhang, L., Stauffer, W. T., Wang, J. S., Wu, F., Yu, Z., Liu, C., Kim, H. J., & Dernburg, A. F. (2023).
1020 Recruitment of Polo-like kinase couples synapsis to meiotic progression via inactivation of CHK-2.
1021 *eLife*, 12, e84492. <https://doi.org/10.7554/eLife.84492>
1022
- 1023 Zhang, L., Stauffer, W. T., Zwicker, D., & Dernburg, A. F. (2021). Crossover patterning through kinase-
1024 regulated condensation and coarsening of recombination nodules. [Preprint]. *bioRxiv*.
1025 <https://doi.org/10.1101/2021.08.26.457865>
1026

1027 **Figure Legends**

1028

1029 **Figure 1. PCH-2 controls the number and distribution of crossovers in similar patterns on**

1030 **multiple chromosomes.** Genetic analysis of meiotic recombination in wildtype and *pch-2* mutants.

1031 DCO indicates double crossovers. Physical and genetic maps of Chromosome I, III, IV and the X

1032 chromosome are depicted to scale. Genetic distance is shown in centimorgans. A * indicates a p-value

1033 < 0.05, a ** indicates a p value < 0.01 and a *** indicates p-value < 0.001.

1034

1035

1036 **Figure 2. PCH-2 prevents exogenous double strand breaks from becoming crossovers in early**

1037 **meiotic prophase. A.** Illustration of the irradiation experiments in control and *pch-2* mutants. Box

1038 indicates late pachytene, the area where GFP::COSA-1 foci are analyzed. **B.** Meiotic nuclei in control

1039 animals and *pch-2* mutants 8 hours post irradiation stained for DAPI (magenta) and GFP::COSA-1

1040 (green). Scale bar is 4 um. **C.** Fraction of meiotic nuclei with less than 6, 6, or greater than 6

1041 GFP::COSA-1 foci in control animals(yellow) and *pch-2* mutants (blue) mutants 8 hours post

1042 irradiation. **D.** Meiotic nuclei in control animals and *pch-2* mutants 24 hours post irradiation with DAPI

1043 (magenta) and GFP::COSA-1 (green). **E.** Fraction of meiotic nuclei with less than 6, 6, or greater than

1044 6 GFP::COSA-1 foci in control animals and *pch-2* mutants 24 hours post irradiation. A *** indicates p-

1045 value < 0.001, and a **** indicates p-value < 0.0001.

1046

1047 **Figure 3. PCH-2 prevents SPO-11-induced double strand breaks from becoming crossovers in**

1048 **early meiotic prophase. A.** Illustration of the SPO-11 depletion experiment to assay GFP::COSA-1

1049 and bivalents in control animals and *pch-2* mutants at different timepoints of auxin treatment. Each

1050 timepoint indicates when SPO-11 is depleted in the germline with auxin induced degradation. Boxes

1051 indicate late pachytene, the area where GFP::COSA-1 foci are analyzed, and diakinesis, where

1052 bivalents are analyzed. **B.** Representative images of meiotic nuclei in control animals and *pch-2*

1053 mutants treated with auxin for 20 hours, stained for DAPI (magenta) and GFP::COSA-1 (green). Scale

1054 bar is 5 um. **C.** Number of GFP::*COSA-1* foci in meiotic nuclei at different timepoints of auxin
1055 treatment in control (blue) and *pch-2* mutants (yellow). Error bars represent standard error of the
1056 mean (SEM). **D.** Oocytes from control animals and *pch-2* mutants stained for DAPI (magenta). Scale
1057 bar is 4um. **E.** Number of DAPI stained bodies in meiotic nuclei at different timepoints of auxin
1058 treatment in control animals and *pch-2* mutants. Error bars represent SEM and a * indicates p-value <
1059 0.05 and a *** indicates p-value < 0.001.

1060

1061 **Figure 4. PCH-2 is required for timely loading and removal of MSH-5 on meiotic chromosomes**

1062 **through its regulation of HIM-3. A.** Representative images of nuclei in different stages of meiotic
1063 prophase in control animals and *pch-2* mutants stained for DAPI (magenta) and GFP::*MSH-5* (green)
1064 Scale bar is 5 um. **B.** Scatter plot showing average GFP::*MSH-5* foci per row of germline nuclei in
1065 control animals (yellow) and *pch-2* mutants (blue) from the transition zone to late pachytene,
1066 normalized to 100. The line represents a rolling average of four rows. **C.** Representative images of
1067 nuclei in different stages of meiotic prophase in *him-3^{R93Y}* mutants (left) and *pch-2;him-3^{R93Y}* double
1068 mutants (right), stained for DAPI (magenta) and GFP::*MSH-5* (green). **D.** Scatter plot showing
1069 average GFP::*MSH-5* foci per row in *him-3^{R93Y}* (brown) and *pch-2;him-3^{R93Y}* mutants (pink) from the
1070 transition zone to late pachytene, normalized to 100. The line represents a rolling average of four
1071 rows. Similar data is provided for a control germline (opaque yellow) for comparison. **E.**
1072 Representative images of meiotic nuclei in control animals and *pch-2* mutants stained for DAPI (blue),
1073 GFP::*MSH-5* (green), and OLLAS::*COSA-1* (red). Yellow circles indicate GFP::*MSH-5* without
1074 OLLAS::*COSA-1*. Scale bar is 4um. **F.** Scatter plot showing average GFP::*MSH-5* (green) and
1075 OLLAS::*COSA-1* (red) foci per row in the last five rows of the germline in control animals and *pch-2*
1076 mutants. The line represents a rolling average of 2 rows. **G.** Swarm plot showing number of
1077 GFP::*MSH-5* foci in control (yellow) and *pch-2* mutant (blue) nuclei with less than 6 OLLAS::*COSA-1*
1078 foci (left) and 6 OLLAS::*COSA-1* foci (right). Error bars represent SEM. A * indicates a p-value less
1079 than 0.05 and a ** indicates a p-value < 0.01.

1080

1081 **Figure 5. PCH-2 is removed when crossovers are designated. A.** Representative images of
1082 meiotic nuclei in *dsb-2* animals 24 hours post L4 and 48 hours post L4 stained for DAPI (magenta),
1083 PCH-2 (red), and GFP::*COSA-1* (green). Scale bar is 4 μ m. **B.** Stacked histograms showing
1084 percentage of PCH-2 positive and negative nuclei with (lime) and without (dark green) GFP::*COSA-1*
1085 foci in *dsb-2* mutants at 24 hours post L4 and 48 hours post L4. **C.** Representative images of meiotic
1086 nuclei in *dsb-2::AID* and *dsb-2::AID;pch-2* mutants treated with auxin and stained for DAPI (magenta)
1087 and GFP::*COSA-1* (green). Scale bar is 5 μ m. **D.** Swarm plot showing the number of GFP::*COSA-1*
1088 foci in *dsb-2::AID* (gray) and *dsb-2::AID;pch-2* (lemon) mutants when treated with ethanol or auxin.
1089 Error bars represent the SEM. A ** indicates a p-value less than 0.01 and a **** indicates p-value <
1090 0.0001.

1091
1092 **Figure 6. PCH-2 and high CHK-2 activity control the fate of early double strand breaks. A.**
1093 Illustration of CHK-2 activity in wildtype and *syp-1^{T452A}* germlines. **B.** Representative images of meiotic
1094 nuclei late pachytene in *syp-1^{T452A}* and *pch-2;syp-1^{T452A}* mutants stained for DAPI (magenta) and
1095 GFP::*COSA-1* (green). Scale bar is 5 μ m. **C.** Swarm plot showing number of GFP::*COSA-1* foci in
1096 control animals (blue), *pch-2* (yellow), *syp-1^{T452A}* (maroon), and *pch-2;syp-1^{T452A}* (light blue) mutants.
1097 Error bars represent SEM. **D.** Oocytes from *syp-1^{T452A}* and *pch-2;syp-1^{T452A}* mutant worms stained for
1098 DAPI (magenta). Scale bar is 4 μ m. **D.** Swarm plot showing number of DAPI stained bodies in control
1099 animals (blue), *pch-2* (yellow), *syp-1^{T452A}* (maroon), and *pch-2;syp-1^{T452A}* (light blue) mutants. Error
1100 bars represent SEM. A **** indicates p-value < 0.0001.

1101
1102 **Figure 7. PCH-2 remodels HIM-3 to disassemble crossover-eligible intermediates, controlling**
1103 **crossover distribution and number. A.** Model for how *pch-2* and *him-3^{R93Y}* mutations genetically
1104 interact to affect the progression of meiotic recombination. HIM-3 adopts the closed conformation
1105 upon binding an interacting protein with a closure motif and its conversion to the extended
1106 conformation is facilitated by PCH-2's remodeling of its HORMA domain. **B.** Model for how PCH-2 and
1107 HIM-3 progressively implement meiotic recombination during different stages of meiotic prophase.

1108

1109 **Supplemental Figure 1: PCH-2 does not regulate GFP::MSH-5 loading and removal through**

1110 **HTP-3. A.** Representative images of nuclei in different stages of meiotic prophase in *htp-3^{H96Y}* and

1111 *pch-2; htp-3^{H96Y}* mutants stained for DAPI (magenta) and GFP::MSH-5 (green) Scale bar in all images

1112 is 5 um. **B.** Scatter plot showing average GFP::MSH-5 foci per row of germline nuclei in *htp-3^{H96Y}*

1113 (blue) and *pch-2; htp-3^{H96Y}* (green) mutants from the transition zone to late pachytene, normalized to

1114 100. The line represents a rolling average of four rows.

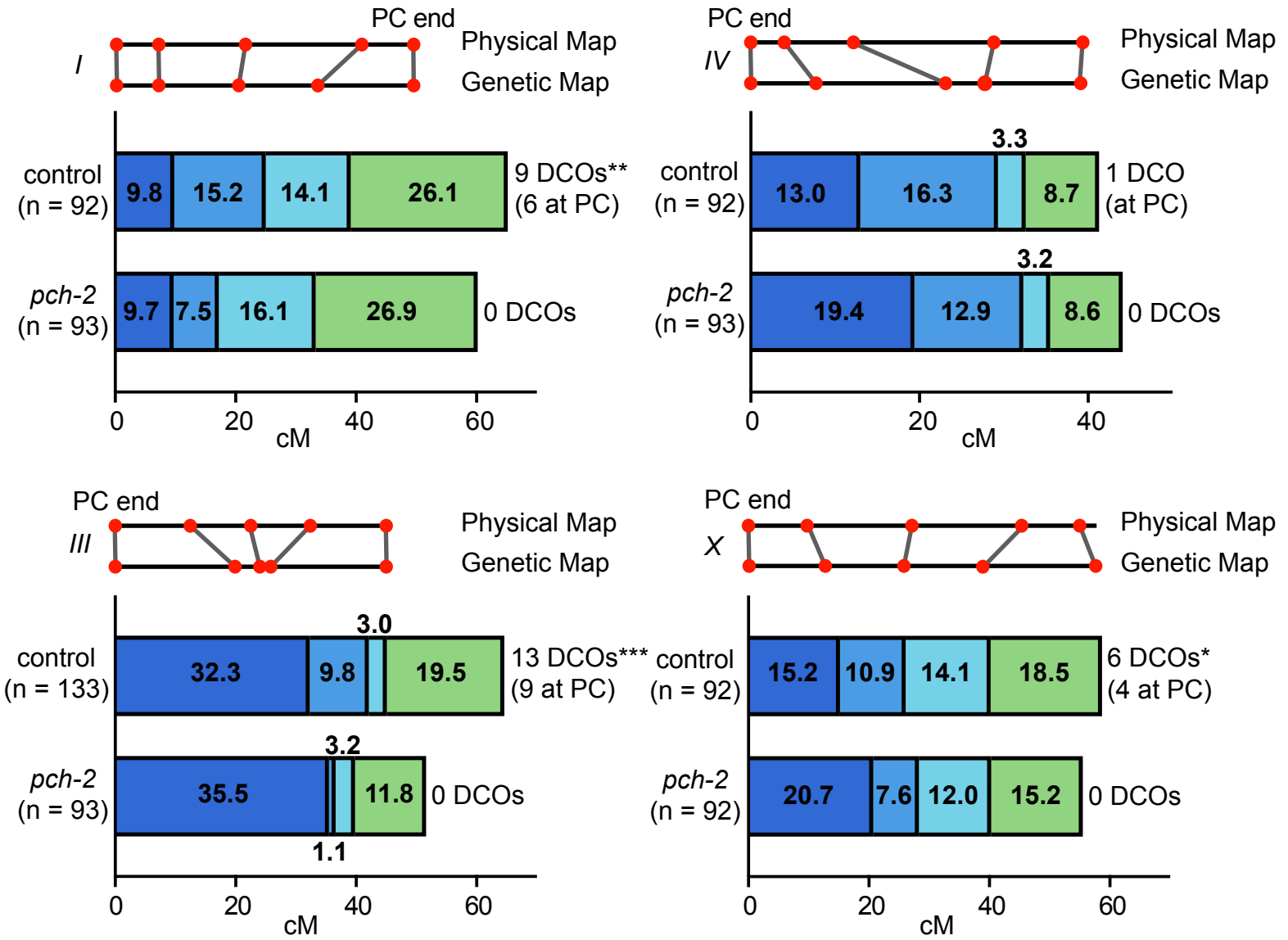
1115

1116 **Supplemental Figure 2: *pch-2* meiotic nuclei with elevated numbers of GFP::MSH-5 foci show**

1117 **defects in crossover assurance.** Gray scale images of control and *pch-2* mutant nuclei stained for

1118 DAPI, GFP::MSH-5 and OLLAS::COSA-1. Scale bar in image is 4 um.

1119



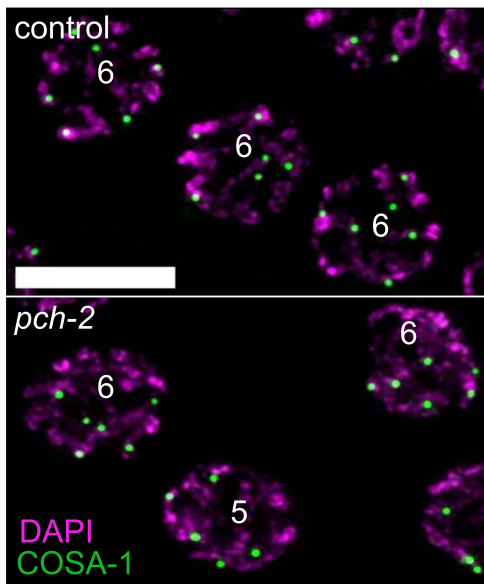
A

bioRxiv preprint doi: <https://doi.org/10.1101/2024.08.13.607819>; this version posted August 13, 2024. The copyright holder for this preprint (which was not certified by peer review) is the author/funder, who has granted bioRxiv a license to display the preprint in perpetuity. It is made available under a [CC-BY-NC 4.0 International license](#).



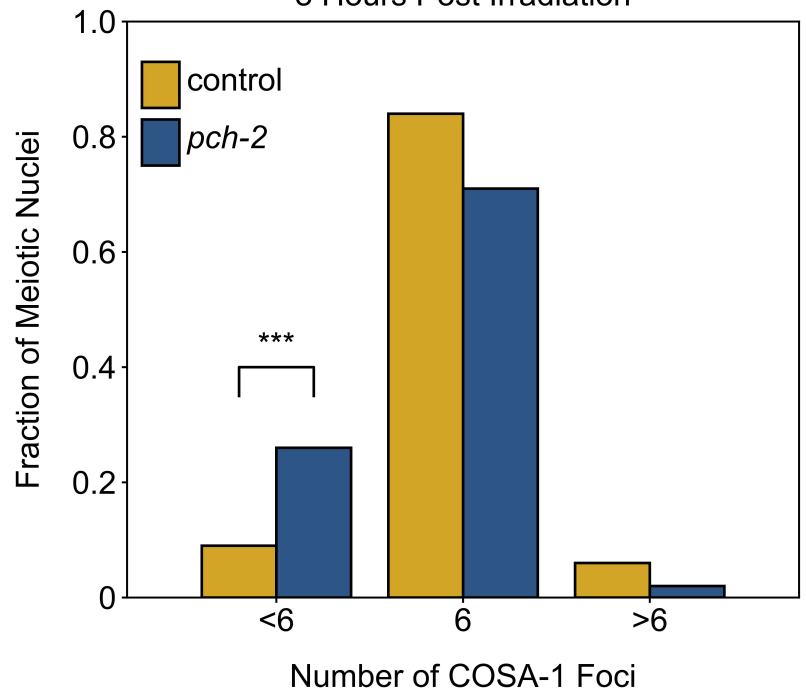
B

8 Hours Post Irradiation



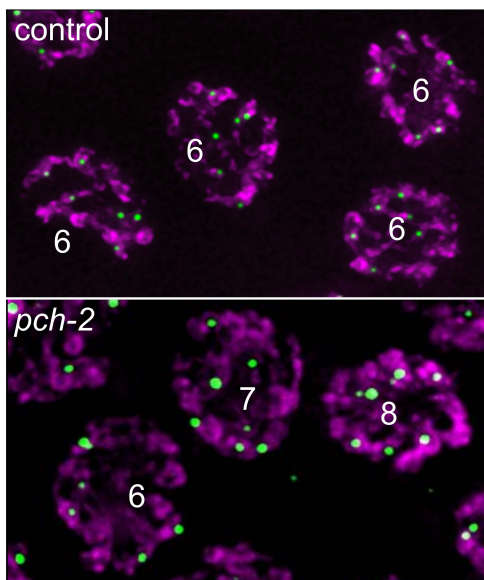
C

8 Hours Post Irradiation



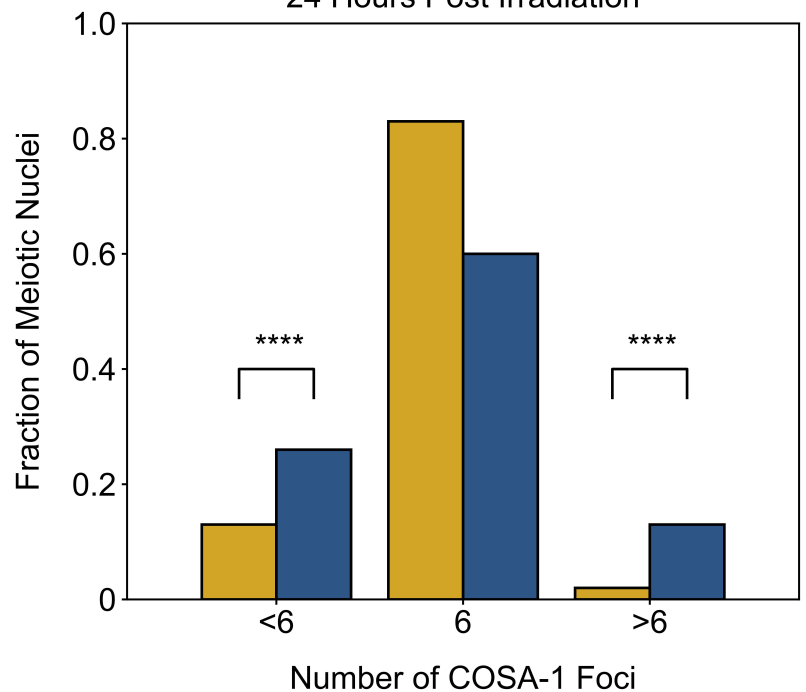
D

24 Hours Post Irradiation



E

24 Hours Post Irradiation



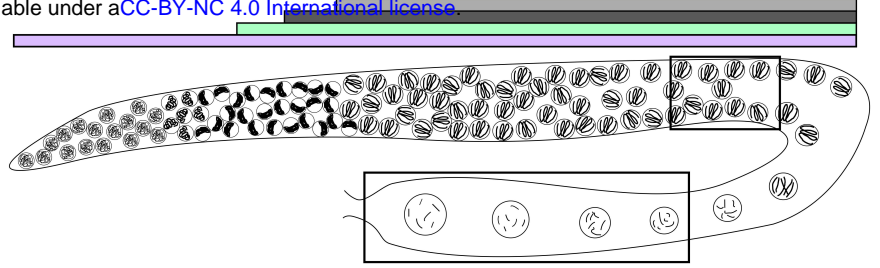
A

Areas of SPO-11 Depletion for COSA-1 and Bivalent Assay

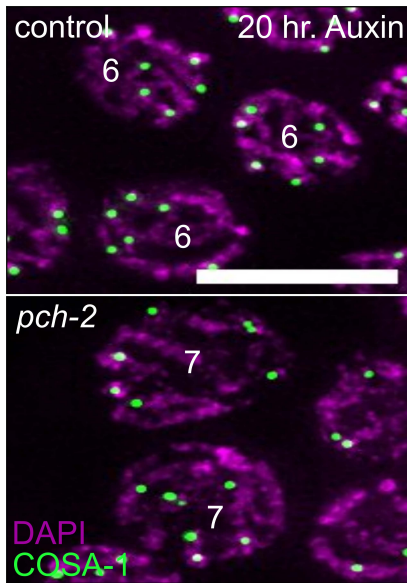
bioRxiv preprint doi: <https://doi.org/10.1101/2024.08.13.607819>; this version posted August 13, 2024. The copyright holder for this preprint (which was not certified by peer review) is the author/funder, who has granted bioRxiv a license to display the preprint in perpetuity. It is made available under aCC-BY-NC 4.0 International license.

Time Points

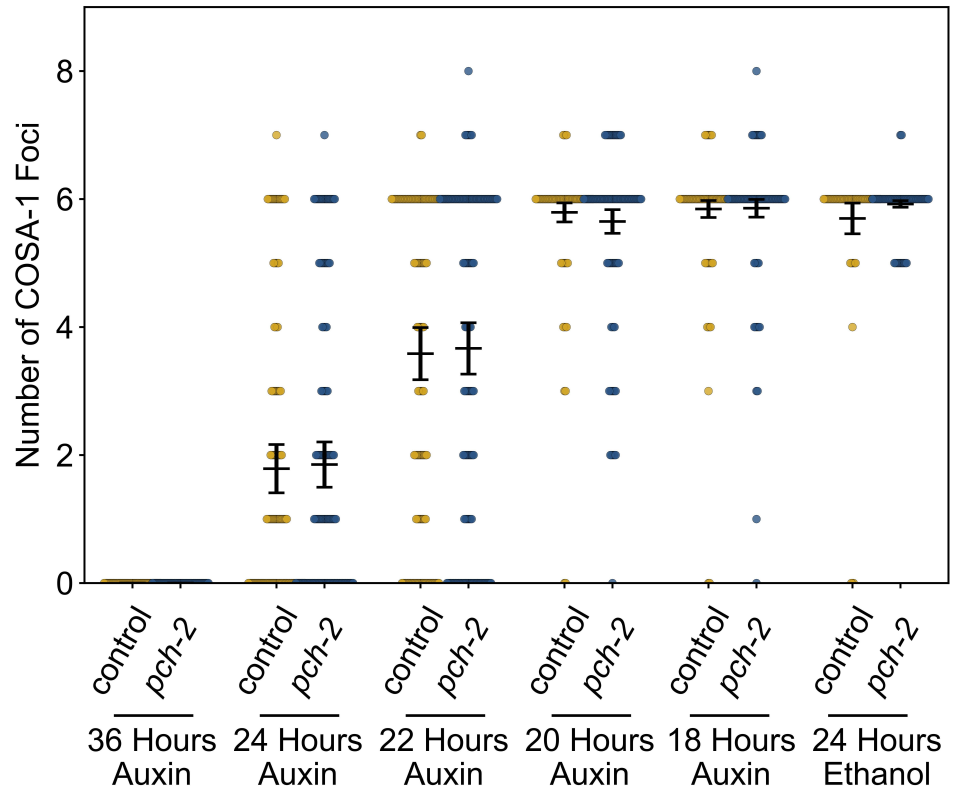
- 36 hr. COSA-1 / 48 hr. DAPI
- 24 hr. COSA-1 / 36 hr. DAPI
- 22 hr. COSA-1 / 34 hr. DAPI
- 20 hr. COSA-1 / 30 hr. DAPI
- 18 hr. COSA-1 / 32 hr. DAPI



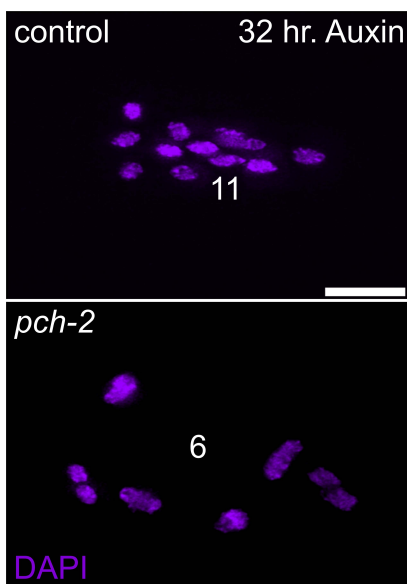
B



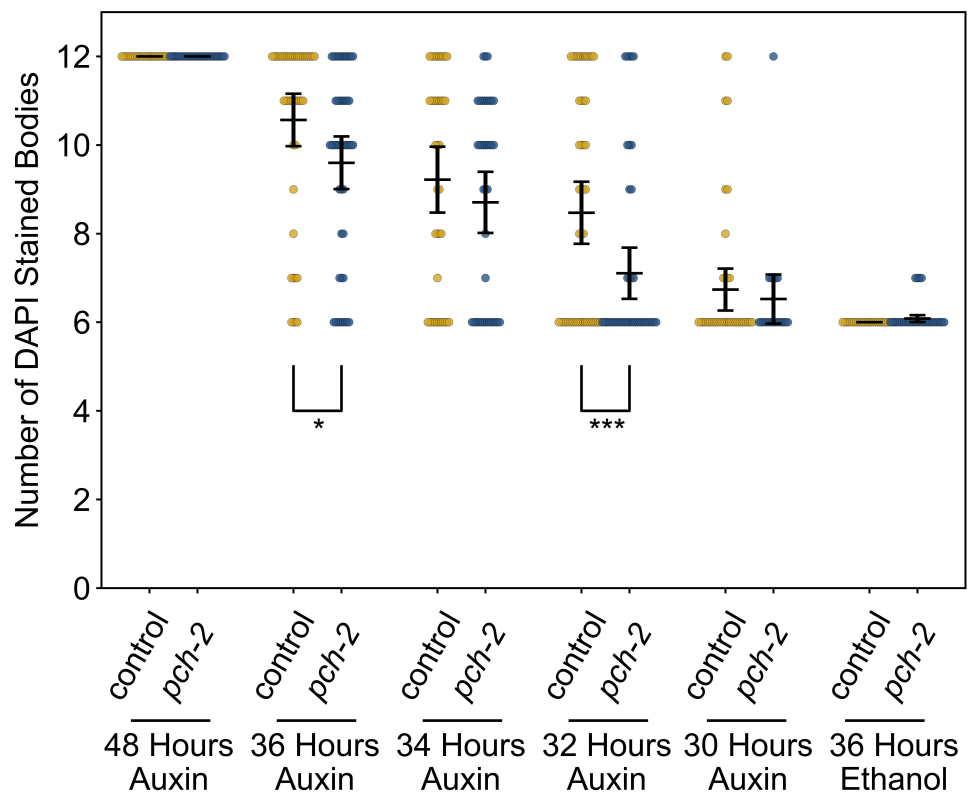
C

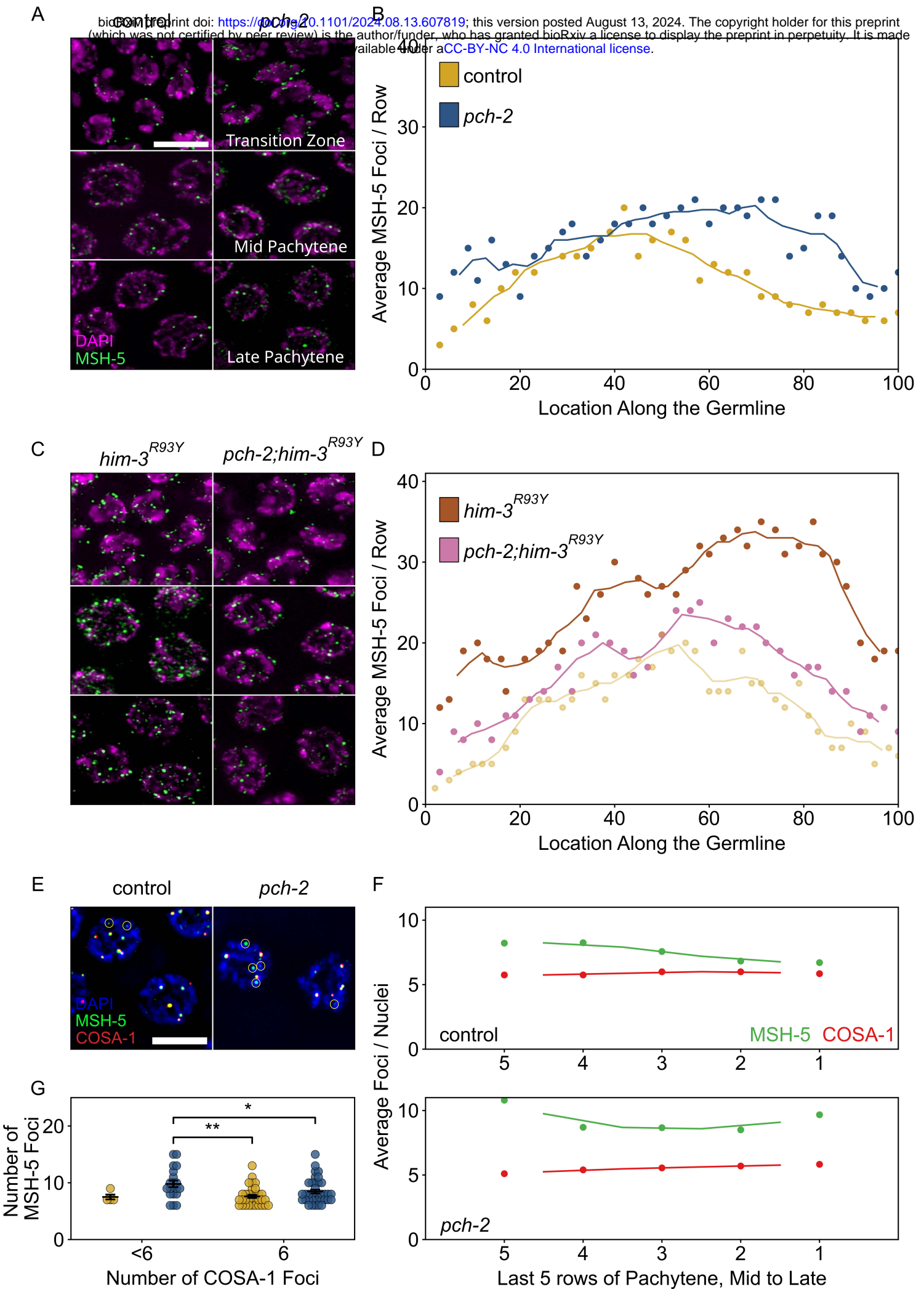


D



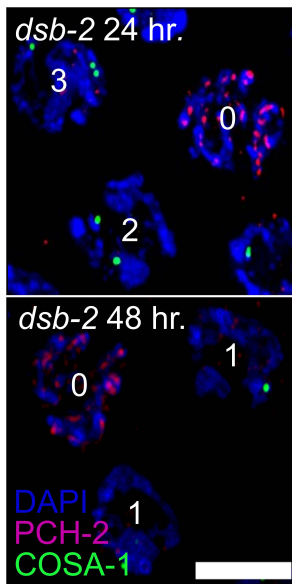
E



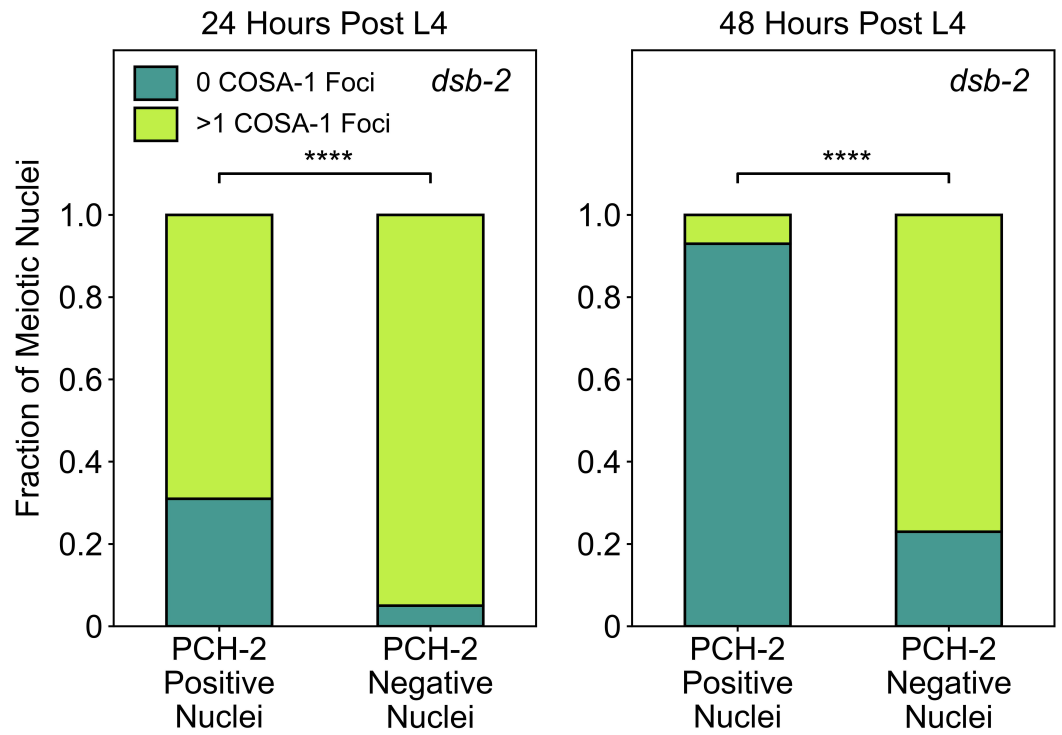


bioRxiv preprint doi: <https://doi.org/10.1101/2024.08.13.607819>; this version posted August 13, 2024. The copyright holder for this preprint (which was not certified by peer review) is the author/funder, who has granted bioRxiv a license to display the preprint in perpetuity. It is made available under aCC-BY-NC 4.0 International license.

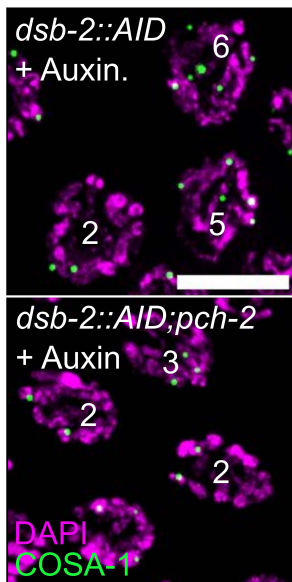
A



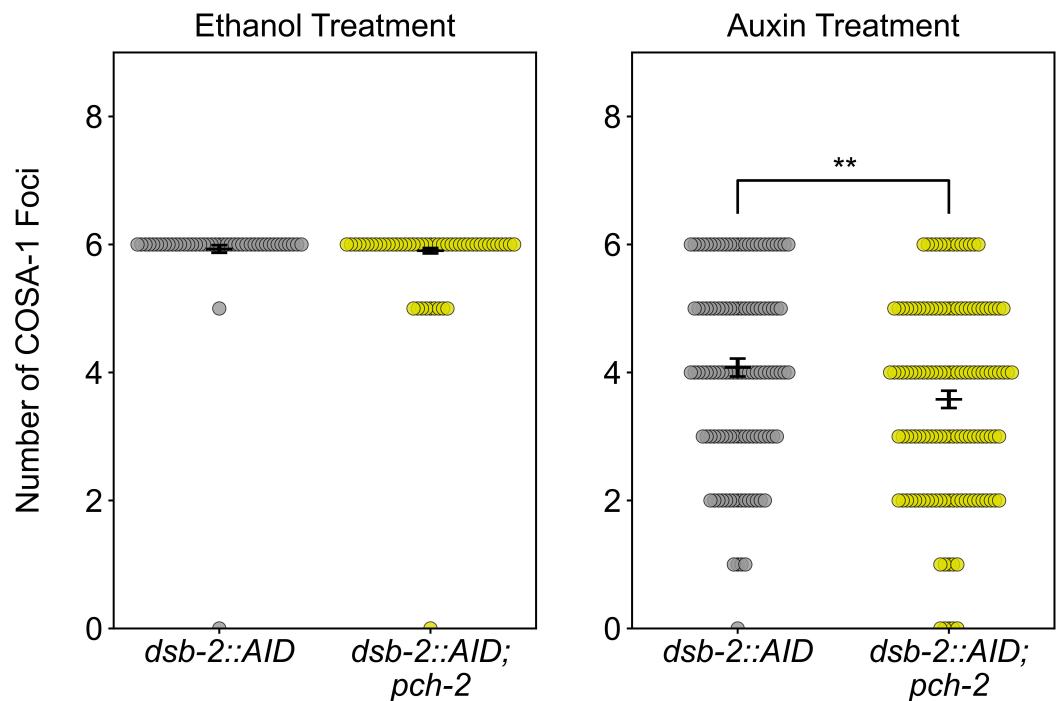
B



C



D

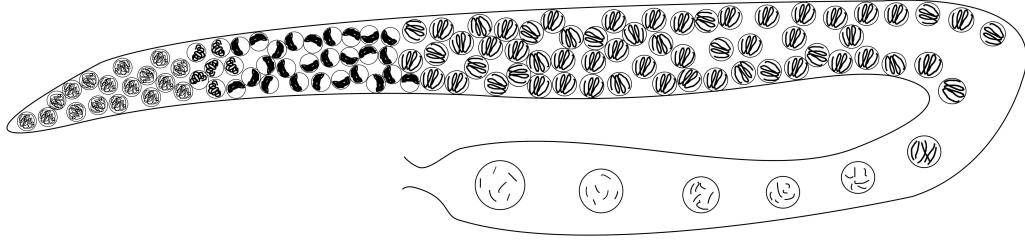


A

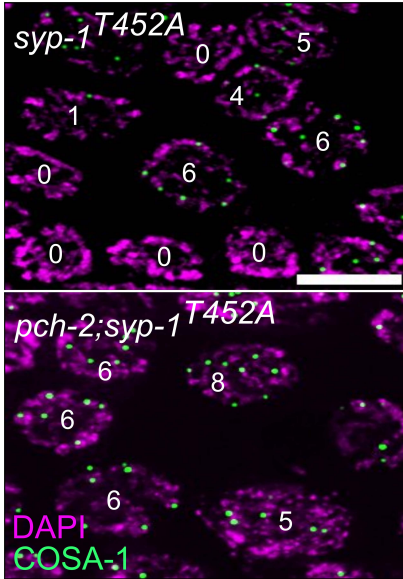
wildtype
 bioRxiv preprint doi: <https://doi.org/10.1101/2024.08.13.607819>; this version posted August 13, 2024. The copyright holder for this preprint (which was not certified by peer review) is the author/funder, who has granted bioRxiv a license to display the preprint in perpetuity. It is made available under aCC-BY-NC 4.0 International license.

syp-1^{T452A}

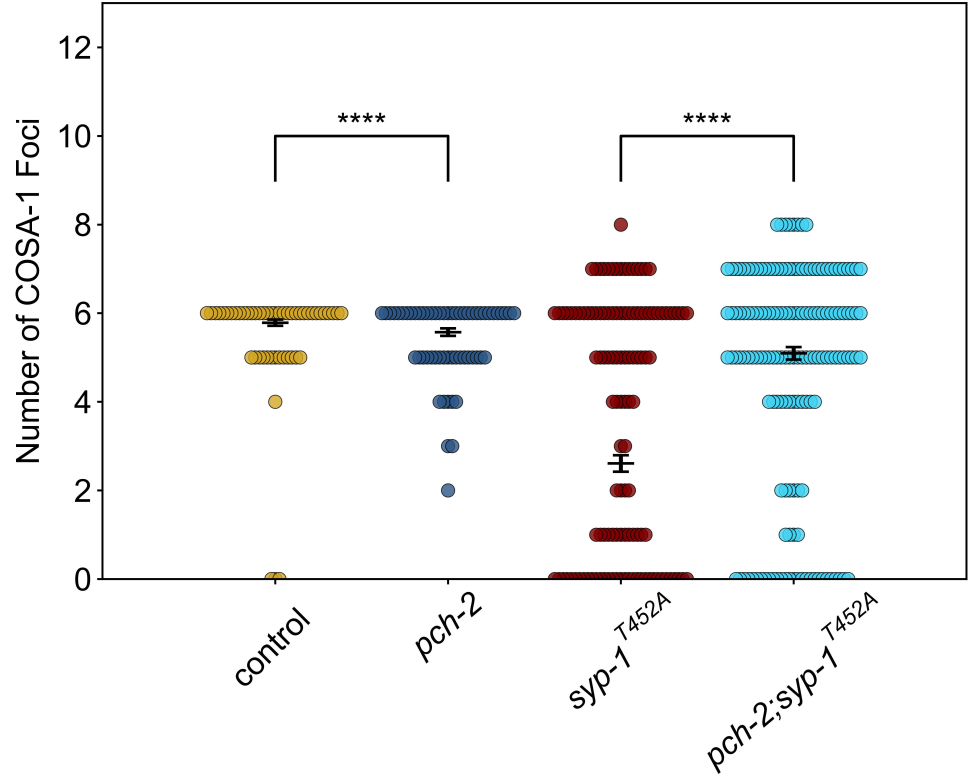
CHK-2 Activity



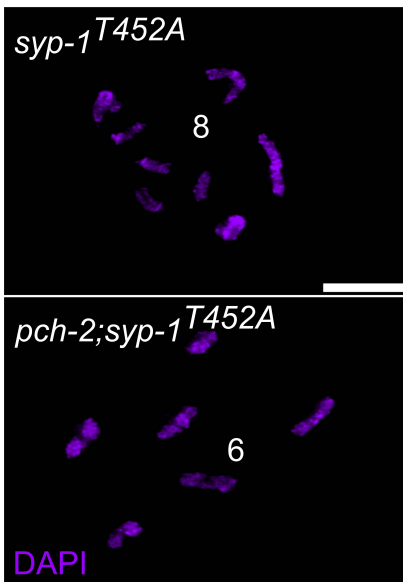
B



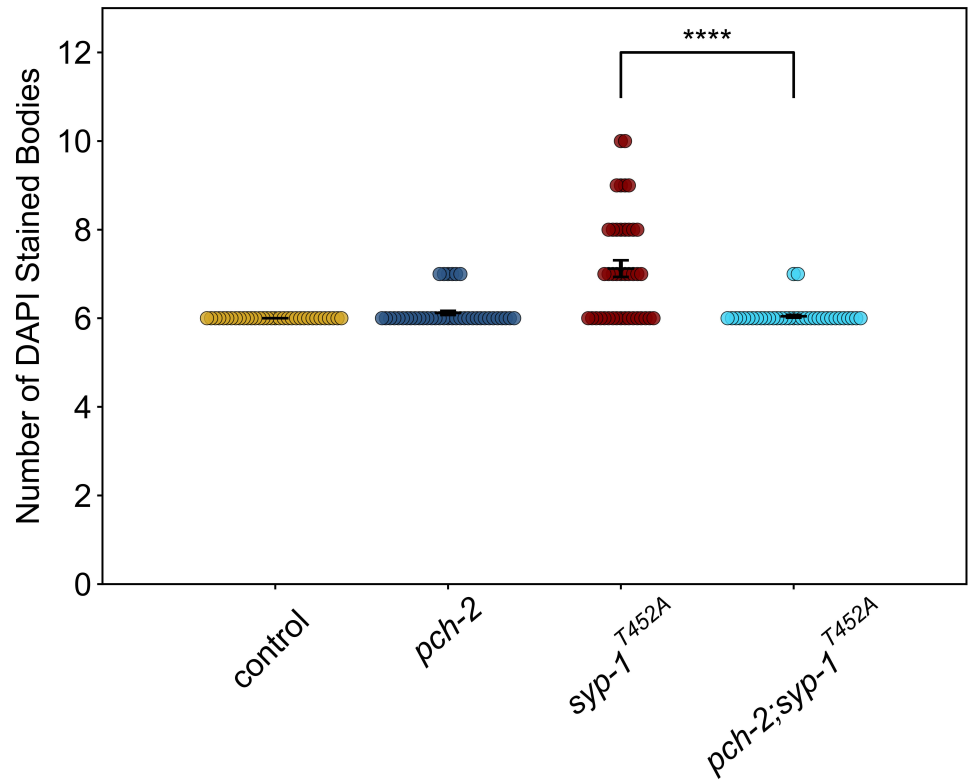
C



D

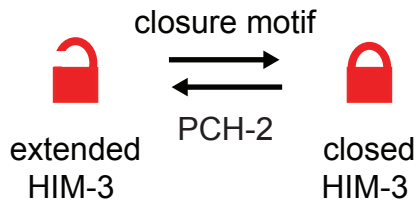


E

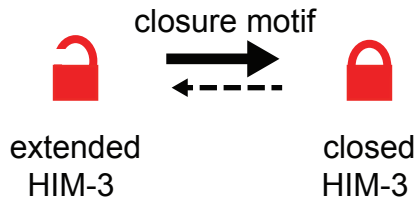


A

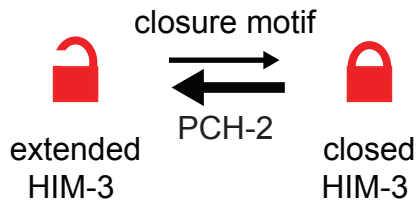
wildtype:



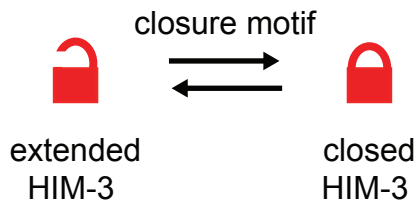
pch-2 mutants:



him-3^{R93Y} mutants:

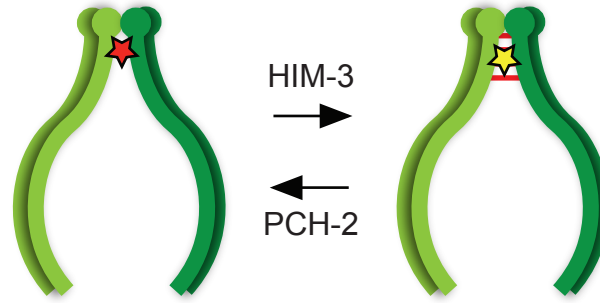


pch-2; him-3^{R93Y} mutants:



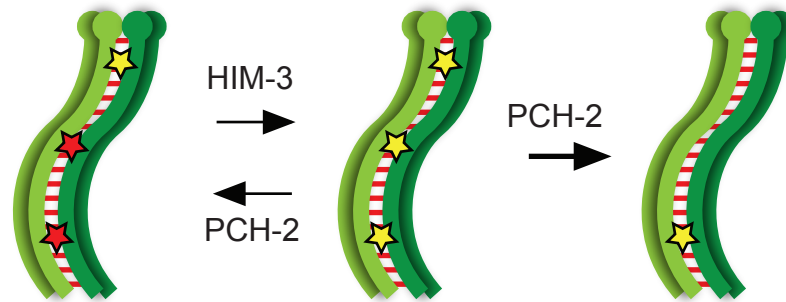
Leptonema/Zygotene

high CHK-2 activity
PCH-2 present as foci
on meiotic chromosomes



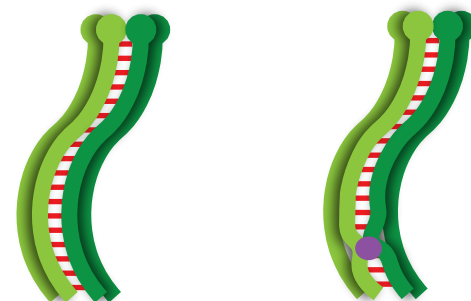
Mid-pachytene:

intermediate CHK-2 activity
PCH-2 localizes to
the synaptonemal complex



no PCH-2

Late-pachytene:
no CHK-2 activity
PCH-2 absent
crossover designation



no
crossover

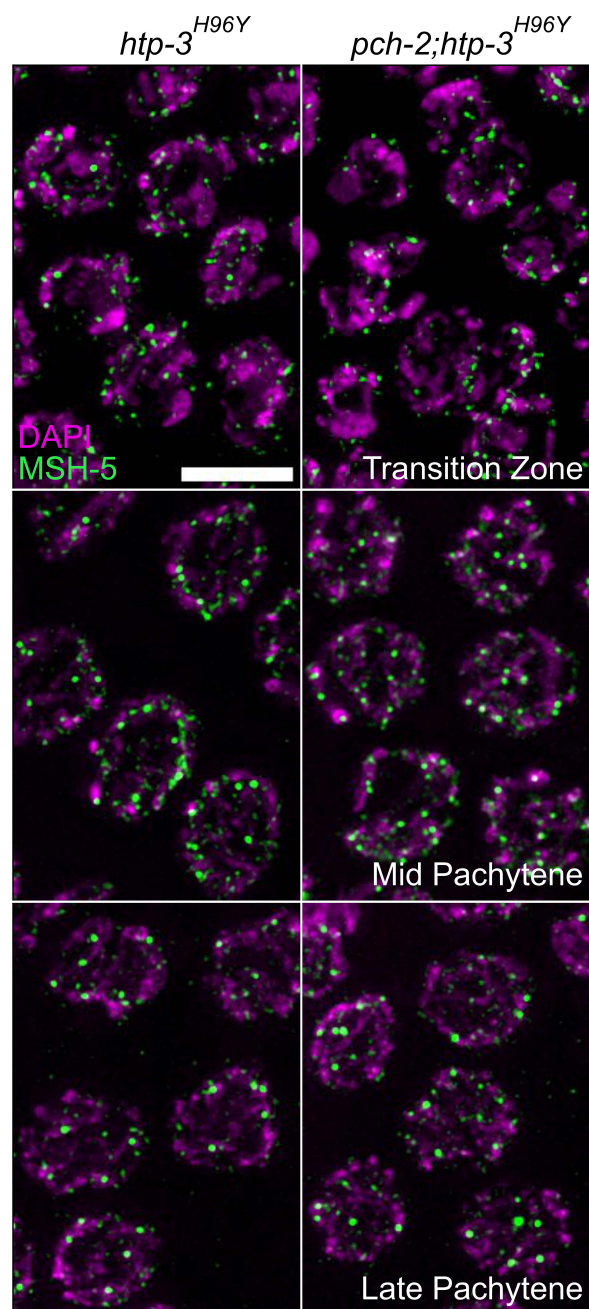
- ★ Double strand break
- ☆ Crossover-eligible intermediate
- Crossover

Supplementary Table 1: Single nucleotide polymorphisms used for recombination assay

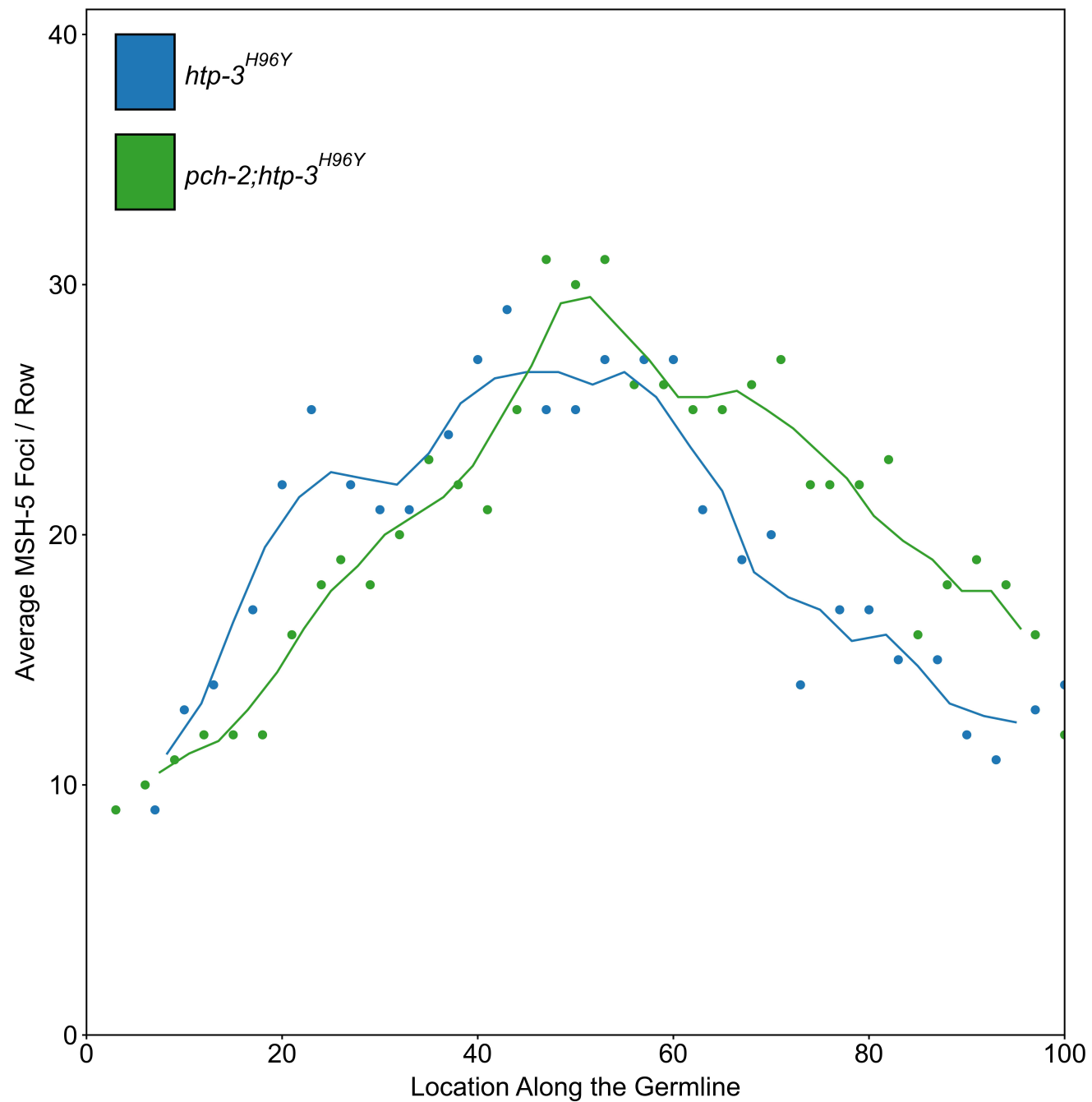
Chromosome and SNP	Primer Name	Primer Genetic Location	Primer Sequence FOR	Primer Sequence REV	Restriction enzyme	N2	HI
IA	F56C11	-19	ATGCCAG TGATAAG GAACGG	TCACATCC CTTGTCGA TGAA	DraI	354, 146	500
IB	Y71G12	-12.3	GACAATG ACCAATA AGACG	GATCCGT GAAATTGT TCCG	BsrI	440, 125	364, 125, 76
IC	K04F10	0.9	ATCATTCT CCAGGCC ACGTTAC	CTGAACTA GTGGAAC AAACCCC	NdeI	594	300, 294
ID	T07D10	13.6	CTTGGTG TGGGGA GAGTATA GG	TTTGTCCG GATTGACT CTGC	Sau3AI	303, 63	207, 96, 63
IE	ZK909	28.8	CACAAGT GGTTTGG AAGTACC G	CAACAAAG GGATAGAT CACGGG	HindIII	450	236, 214
IIIA	pkP3081	-26.98	AGCAAGA ATGAGCC GATTG	GTCGGCC GTTTTCAA ATAACTG	TaqI	222, 149	195, 145, 27
IIIB	pkP3095	-5.12	TCTCGTC AATTGTC GCCTG	TTATTTGC AATCCAAC GGC	ApoI	308	168, 140
IIIC	pkP3101	-0.9	CCAAGTG CAAATA TGGTGC	ATAAACAA TTTCAGTG CCGC	HinfI	495	282, 213
IIID	pkP3035	0.9	CGTAAAC TACCAA CTCGGTG	GGTCTACT ACAACAT ACAGGC	Eco0109I	732	419, 313
IIIE	pkP3080	21.29	CGGTGGT GGTAAAA GTGTAAC	CAACATTC AGGCTGT GCTTTCC	Hpy188III	365, 76, 68, 35	241, 124, 76, 68, 35
IVA	F56B3	-24	TGATGGT GTGTCTG CGTACC	AGAGCTG GAGAGCA CGGATA	DraI	301, 128, 71	429, 71
IVB	F52C12	-14.9	ACATTTA GTCACGC GTAGGG	GCCCGAA TCTAGCAC ATAAG	HpaII	191, 137, 22	328, 22
IVC	B0273	1.8	AATACAG CAGTCGT TCCGTTT	TGAACTTC ATGAACCA GCTTG	DraI	288, 144	432

IVD	K10D11	6.7	GATTATTT CAGAGGA GCAGAGC	CATAGCAC GTGGAATA ACCAC	HindIII	420	245, 175
IVE	T02D1	16.8	TGCTTAA AGTCATC GTGTCCA C	TGTAAACC GTATCGAA TCCGAC	EatI	174, 235	408
XA	pkP6139	-19.97	AAGAGTG AACCTTT TCCGTGA G	TGATGCAA TTTATACA CACGCC	MseI	401, 31	279, 122, 31
XB	pkP6120	-10.46	TCGTGGC ACCATAA AAGTG	GATTCAGA TCAAACAG AGGTGG	DraI	243	128, 115
XC	pkP6157	-0.14	GGGGTAT AATGAAC CAACCTG	TGTAGGAA CCGTTTGT TTCTTC	ApoI	261, 48	150, 111, 48
XD	pkP6161	9.38	ATCGACC CCAACAA TGAC	TCCGTCAT CCAAATCT CCG	AseI	542	287, 255
XE	pkP6170	24.07	CGCTGTC ACAATCT CTAAAAT G	AAACCCTC CCCCTTT GTTGTC	ApoI	249, 118, 56	197, 118, 56, 52

A



B



A

